Title

Pyrolysis Pathways of the Furanic Ether 2-Methoxyfuran

Journal

The Journal of Physical Chemistry A, 119(39)

ISSN

1089-5639

Authors

Urness, Kimberly N

Guan, Qi

Troy, Tyler P

et al.

Publication Date

2015-10-01

DOI

10.1021/acs.jpca.5b06779

Peer reviewed

Pyrolysis Pathways of the Furanic Ether 2-Methoxyfuran

Kimberly N. Urness,[†] Qi Guan,[†] Tyler P. Troy,[‡] Musahid Ahmed,[‡] John W. Daily,[*,†] G. Barney Ellison,[*,¶] and John M. Simmie[*,§]

Department of Mechanical Engineering, University of Colorado, Boulder, CO 80309-0427, USA, Chemical Sciences Division, LBNL MS 6R-2100, Berkeley, CA 94720, USA , Department of Chemistry and Biochemistry, University of Colorado, Boulder, CO 80309-0215, USA, and Combustion Chemistry Centre, School of Chemistry, National University of Ireland, Galway, Ireland

E-mail: john.daily@colorado.edu; barney@jila.colorado.edu; john.simmie@nuigalway.ie

Abstract

Substituted furans, including furanic ethers, derived from nonedible biomass have been proposed as second-generation biofuels. In order to use these molecules as fuels it is important to understand how they break apart thermally. In this work a series of experiments were conducted to study the unimolecular and low-pressure bimolecular decomposition mechanisms of the smallest furanic ether, 2-methoxyfuran. Electronic structure (CBS-QB3) calculations indicate this substituted furan has an unusually weak $O-CH_3$ bond, approximately 190 kJ mol^{-1} (45 kcal mol^{-1}), thus the primary decomposition pathway is through bond scission resulting in CH_3 and 2-furanyloxy (O-C_4H_3O) radicals. Final products from the ring opening

*To whom correspondence should be addressed
[†]Department of Mechanical Engineering
[‡]LBNL
[¶]Department of Chemistry
[§]National University of Ireland, Galway

of the furanyloxy radical include 2 CO, HC≡CH and H. The decomposition of methoxyfuran is studied over a range of concentrations (0.0025−0.1%) in helium or argon in a heated silicon carbide (SiC) microtubular flow reactor (0.66−1 mm i.d, 2.5−3.5 cm long) with reactor wall temperatures from 300 to 1300 K. Inlet pressures to the reactor are 150 to 1500 Torr and the gas mixture emerges as a skimmed molecular beam at a pressure of approximately 10 μTorr. Products formed at early pyrolysis times (100 μs) are detected by 118.2 nm (10.487 eV) photoionization mass spectrometry (PIMS), tunable synchrotron VUV PIMS and matrix infrared absorption spectroscopy. Secondary products resulting from H or CH_3 addition to the parent, and reaction with 2-furanyloxy were also observed and include CH_2=CH-CHO, CH_3-CH=CH-CHO, CH_3-CO-CH=CH_2 and furanones; at the conditions in the reactor we estimate these reactions contribute to at most 1-3% of total methoxyfuran decomposition. This work also includes observation and characterization of an allylic lactone radical, 2-furanyloxy (O-C_4H_3O), with the assignment of several intense vibrational bands in an Ar matrix, an estimate of the ionization threshold and photoionization efficiency. A pressure-dependent kinetic mechanism is also developed to model the decomposition behavior of methoxyfuran and provide pathways for the minor bimolecular reaction channels that are observed experimentally.

Introduction

Alkylated furans and furanic ethers are among a variety of molecules derived from non-edible biomass that offer a renewable path to biofuels and platform chemicals. Reviews by Haro et al. discuss potential routes for biochemical refineries, while Lange, Dutta, Van Putten and colleagues focus on the platform chemicals furfural and hydroxymethylfurfural as gateway molecules to a variety of potential biofuels.[1] Despite the recent interest in these oxygenated species, the combustion and pyrolytic behavior of many of them are not well-known; an objective of this work is to remedy this deficit in regards to the title compound, the simplest furanic ether.

Methoxyfuran was included in a study of several aromatic compounds relevant to coal-combustion by Bruinsma et al.[2] In this study they measured the disappearance of methoxyfuran as a function of

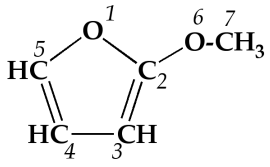

Scheme 1: The chemical structure of 2-methoxyfuran (2-MeOF) and the numbering scheme used throughout the text

temperature in a coiled quartz flow reactor operated at 0.125 MPa (938 Torr), a residence time of 5 s and a sample concentration of at most 500 ppm (0.05%) in argon. The primary products detected by gas chromatography at 10% conversion included CO, CO_2 and trace amounts of other species. The authors noted that this molecule was "abnormally reactive" compared to other substituted heterocycles; the observed onset for decomposition was about 300 K lower than for other molecules included in the study. A recent quantum chemical study[3] showed that this was an accurate finding, and that the abnormal reactivity was largely due to the very weak bond between the methyl group and the O-atom, which at 190 kJ mol^{-1} (45 kcal mol^{-1}) is one of the weakest known C−O bonds[4] and is about 200 kJ mol^{-1} weaker than the ring C−H bonds in 2-methoxyfuran. Together with computed rate constants for methyl attack on the parent compound, a simplistic mechanism was able to re-interpret the original experiments in a satisfactory manner; however, the absence of detail beyond the decrease in reactant concentration as a function of temperature was a hindrance in understanding the behavior of this interesting system. Except for these initial experiments of this reactive molecule, it appears no additional pyrolysis or combustion studies have been performed.

The computational study of Simmie et al.[3] predicts that the dominant pathway for thermal decomposition is loss of CH_3 to produce the allylic lactone, 2-furanyloxy radical (γ-butryolactonyl radical, m/z 83), as shown in Scheme 2. The structure and thermochemical properties of 2-methoxyfuran and the radicals formed by loss of hydrogen atoms have also been examined computationally by Hudzik and Bozzelli.[5]

To date there is no experimental evidence for the 2-furanyloxy radical, however the structure and stability of this allylic lactone have been discussed in several computational studies. The 2-furanyloxy radical is predicted to be an intermediate in the oxidation of 2-furanyl radical[6] and

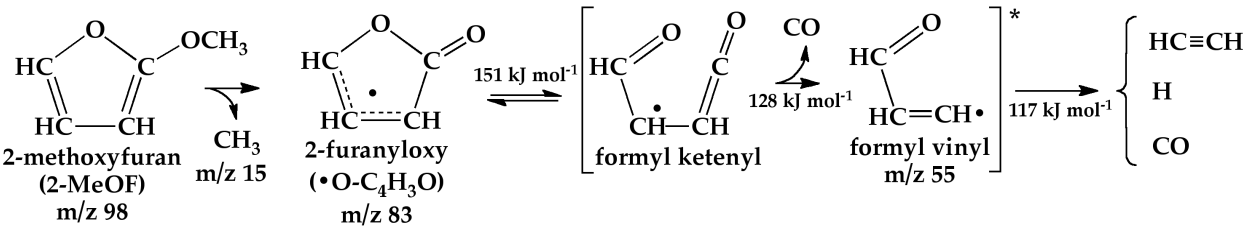

Scheme 2: Primary unimolecular decomposition pathway of 2-methoxyfuran, including the lowest calculated reaction barriers.[3]

also a minor, high-energy channel intermediate in the oxidation of phenyl radical.[7] Prior to these studies, Yamamoto et al.[8] calculated the cyclization of the formyl ketenyl radical (4-oxo-but-3-enal-2-yl) in Scheme 2 to 2-furanyloxy.

This work documents a series of experiments using a silicon carbide (SiC) microreactor to identify the products from the unimolecular and low-pressure bimolecular decomposition mechanisms of the simplest furanic ether, 2-methoxyfuran. Also included is the first experimental characterization of 2-furanyloxy radical by assignment of several infrared vibrational bands in an Ar matrix, in addition to the ionization threshold and photoionization efficiency. These assignments are supported by calculations of the harmonic vibrational frequencies and ion properties. The microreactor offers a short residence time (100 μs) coupled with the sensitive diagnostics photoionization mass spectrometry (PIMS) and matrix isolation infrared absorption spectroscopy.[9] The short residence time allows for rapid heating and identification of the first pyrolysis products, eliminating most, if not all, secondary reactions. Since the only pyrolysis experiments of methoxyfuran[2] were recorded at long reaction time scales, no detection of the organic radicals or other reactive intermediates were possible; the use of the microreactor in the present study enables identification of these elementary reaction steps.

Experimental Methods

Microreactor and Sample Preparation

The microreactor consists of a resistively heated silicon carbide (SiC) tube, 2.5−3.8 cm in length, 0.66−1 mm i.d. and 2 mm o.d. The heated length is about half to two-thirds the full length of the reactor, with the temperature of the outer wall measured by a tungsten/rhenium Type C or a chromel-alumel Type K thermocouple.[10] The maximum operable temperature of the microreactor is about 1700 K, but due to the reactive nature of methoxyfuran, the temperature range was limited to 300−1300 K to allow detection of reactive intermediates.

The flow through the reactor was controlled with either a pulsed valve (Parker General Valve, series 9) or a mass flow controller (MKS P4B 0-200 sccm N_2). A brief summary of the fluid dynamics within the continuous flow reactor is presented in the Reactor Modeling section, with a more detailed description available in Guan et al.[9] The downstream pressure for all reactor assemblies is maintained at approximately 1−10 μTorr. The total backing pressure to the pulsed valve is about 1500 Torr for He PIMS and 800 Torr for experiments in Ar. The inlet pressure to a 300 K continuous flow reactor is about 100 Torr and increases linearly to 200 Torr with a reactor temperature of 1200 K. Estimates of the pressure and temperature profiles of the gas within the reactor based on computational fluid dynamics are shown in Figure 1.

In addition to the temperature and pressure profiles, another important reactor operating condition is the residence time in the heated portion. The longer the residence time, the more possibilities there are for radical-radical reactions and radical addition or abstraction reactions with the precursors under investigation, which greatly complicates the analysis of the desired unimolecular processes. One way to assess the possibility of bimolecular reactions is based on collisions. Considering the single particle collisional frequency:

$$Z_{ii} = \sqrt{2} N_i \sigma_i \sqrt{\frac{8 k_B T}{\pi m_i}} \quad \text{(collisions s}^{-1}\text{)} \tag{1}$$

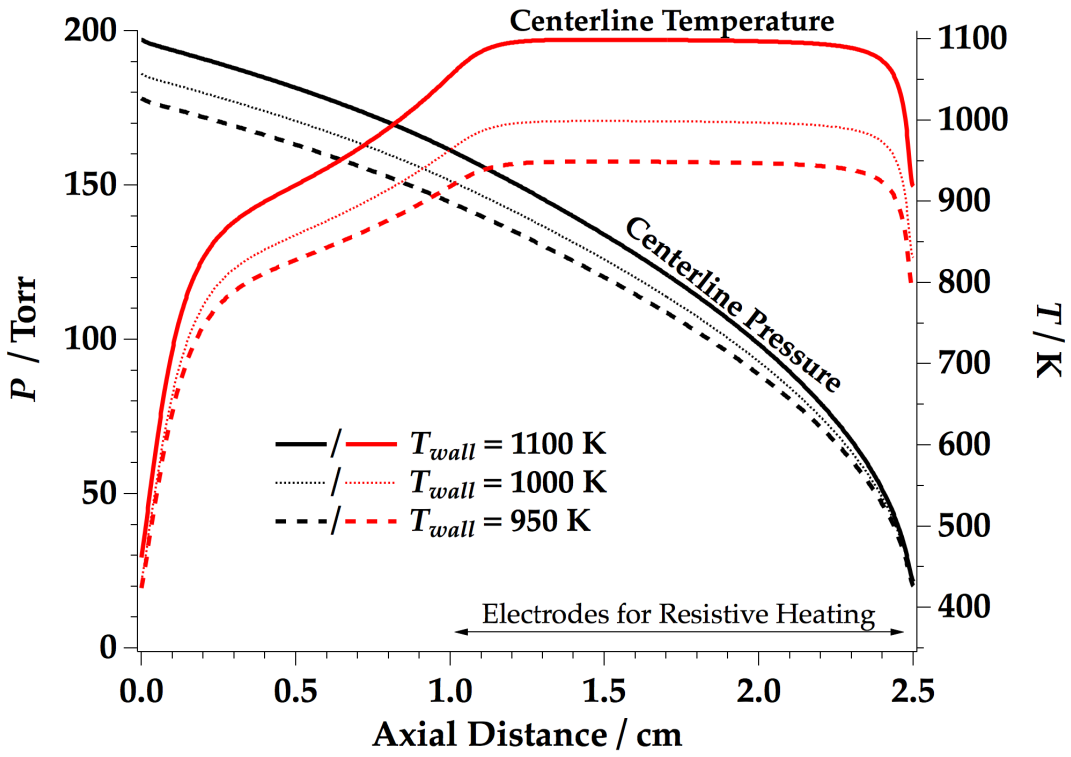

Figure 1: Simulated profiles (see Ref. 9) of the helium carrier gas pressure and temperature along the length of the reactor as function of external wall temperature ($\dot{m}_{\mathrm{He}}$ = 280 sccm).

where N_i is the number of species i per unit volume, σ_i is the collision cross-section, k_{B} is the Boltzmann constant (1.38×10^{-23} J K^{-1}), T is the temperature and m_i is the mass of species i. The pressure, P_i can be related *via* the Ideal Gas Law as $P_i = N_i k_B T$. Therefore with an intermediate temperature (T) and pressure (P) of 1200 K and 200 Torr (26.7 kPa), the collisional frequency in the reactor (Z_{ii}) is on the order of 1000 collisions μs^{-1} (assuming σ = 0.4 nm^2 and m_i = 0.04 kg mol^{-1}). Incorporating a dilution of 0.01% (a partial pressure of 0.02 Torr) and a residence time of 50−100 μs, a rough estimate of the collisions between potentially reactive species is on the order of 5−10 collisions. Reactions that occur at the gas kinetic rate could be influential at these conditions, but most rates will be at least an order of magnitude lower and therefore will not be significant compared to the unimolecular reaction scheme of interest. Decreasing the residence time in the reactor is not a viable way to avoid bimolecular reactions, because it is essentially a fixed experimental parameter due to limited pumping capabilities, so instead this task is accomplished

through dilution. In general, the product distributions may differ slightly between the different carrier gases and flow conditions because of variations in the pressure/temperature time-history (as thoroughly discussed in Guan et al.[9]); however, the products themselves remain consistent.

Dissolved water was removed from the methoxyfuran sample (Aldrich, $\geq$ 97%) with anhydrous $MgSO_4$ and the dried sample was degassed using a liquid nitrogen freeze-pump-thaw cycle prior to preparing gaseous mixtures in helium or argon. The reactant mixtures for the pulsed experiments ranged from $0.03\%-0.1\%$ in He or Ar carrier gas. The reactant mixtures prepared for the experiments in a continuous flow reactor are between $0.0025-0.01\%$ methoxyfuran in helium, about an order of magnitude lower than those for pulsed experiments, due to a longer effective residence time in this style reactor compared to the pulsed reactor (more detailed descriptions of the reactor assemblies are described in Refs. 11 and 12).

Photoionization Time-of-Flight Mass Spectrometry

Two types of photoionization mass spectrometry (PIMS) experiments are reported here with more detailed descriptions of these diagnostic techniques reported elsewhere.[11,13] Briefly, one set of experiments is operated with pulsed flow through a heated SiC reactor and pyrolysis products ionized by fixed wavelength (λ_0 = 118.2 nm, 10.487 eV) vacuum ultraviolet (VUV). Ions are detected with a microchannel plate and the spectra collected with a digital oscilloscope, averaging 1000 individual mass spectra per reported spectrum. Another set of PIMS spectra are collected at the Chemical Dynamics Beamline (9.0.2) of Lawrence Berkeley National Laboratory's Advanced Light Source (ALS) using a reactor operated with continuous flow and pyrolysis products ionized by tunable VUV in the range of 7.85 to 15.5 eV. The spectra from these experiments are a composite of 100,000 to 500,000 individual mass spectra at each photon energy. Photoionization efficiency (PIE) curves for a given mass were obtained by plotting the summation of the background corrected ion signal in an appropriate mass range versus the selected photon energy, normalized by the photon flux measured by an SXUV photodiode with a NIST calibrated energy-dependent efficiency. Due to unreliable measurements during the present study, the PIE curves reported here

were corrected using photodiode measurements from a set of experiments on the same end-station recorded one month prior. In addition, a thicker Type-K thermocouple (chromel-alumel, diameter 0.01 in) was used for one set of continuous flow experiments at the ALS; the potential impacts of these measurements are addressed in the text.

Matrix Isolation Infrared Absorption Spectroscopy

Infrared spectroscopy in an argon matrix is also used as a complement to the PIMS, providing structural information for the pyrolysis products and differentiating thermal products of identical mass. The molecular beam formed at the reactor exit is aimed at a cold infrared transparent window and the products, now trapped in frozen argon, are detected by FT-IR spectroscopy.

A two-stage closed-cycle helium cryostat (APD Cryogenics, 60 Hz and 2.5 W cooling capacity at 20 K) cools a CsI window to about 10 K. Reactant mixtures are prepared in a glass 1.2 L reservoir upstream of the reactor in concentrations of $0.04-0.1\%$ 2-methoxyfuran in Ar. Typical deposition rates through the pulsed valve operated at 20 Hz are $0.8-1$ Torr min^{-1} from the reservoir (equivalent to $3-3.6$ mmol hr^{-1}), with approximately $3-6.5$ mmol total deposited onto the cold window. The vibrational spectra are measured using a commercial infrared spectrometer equipped with a liquid N_2 cooled mercury/cadmium/telluride detector (MCT/A, $4{,}000-600$ cm^{-1}). A background scan was taken approximately 1 to 2 hours prior to the sample scan; all reported spectra averaged 500 scans at 0.25 cm^{-1} resolution.

Computational Methods

Quantum Chemical Calculations

The application Gaussian-09 was employed to compute the geometries, harmonic frequencies and energetics of all species, including transition states, reported in this study.[14] The majority of the calculations used the model chemistry CBS-QB3 since this composite method[15] was used previ-

ously to determine the potential energy diagram for the thermal decomposition of the 2-furanyloxy radical.[3] Additional results were obtained with the density functional M06-2X[16] and the basis set 6-311++G(d,p). Specified transition states were connected to specific reactants and products *via* intrinsic reaction coordinate calculations.[17] The adiabatic ionization energies (see Table 1) were computed by a number of composite methods including CBS-QB3, G3[18] and CBS-APNO.[19] For the title compound in its lowest energy conformation, with the methyl group *cis* to the carbon-carbon double bond in the ring,[5,20] the ionization energy is 7.93 eV,[21] with the less-stable *skewed* or *trans* conformer (^{1}A), O-C-O-CH_3, only slightly less at 7.79 eV. The ionization energy of furanyloxy radical (see Scheme 2) is 8.23 eV, while the formyl ketenyl radicals, which can be categorized according to the dihedrals O=C-C-C and CCCC since C=C=O is always linear, ionize below 8 eV and are summarized in Table 1.

Reactor Modeling

In order to make quantitative measurements of the chemical reactions that occur within the microreactor a detailed understanding of the flow fields inside the reactor is required. The small size of the reactor makes it difficult to insert sampling probes or gain optical access, and therefore the thermodynamic conditions within the reactor were simulated using computational fluid dynamics.[9] The flow was determined by solving the two-dimensional axisymmetric Navier-Stokes equations in addition to the heat equation to account for the heat transfer from the reactor walls. The defined boundary conditions, measured experimentally, include the temperature of the reactor's outer wall, the mass flow rate and the inlet pressure to the reactor. Through simulation it was found that an important operating condition is to maximize the pressure drop within the reactor in order to maintain a continuum flow (which can be modeled by Navier-Stokes relations) and ensure that the flow chokes (*i.e.* the local flow velocity reaches the local speed of sound) to produce an underexpanded supersonic jet downstream, an important characteristic for molecular studies (see for example Anderson et al.[42]). The important results obtained from these simulations are the temperature and pressure profiles of the internal gas as a function of external wall temperature, with the centerline

Table 1: Chemical formulas, common names and nominal masses of species referred to in the kinetic mechanism and throughout the text. Also included are the experimentally measured or calculated ionization energies.

m/z	Formula	Species	IE (eV)	Ref.
1	H	hydrogen atom	13.59844 ± 0.00001	[22]
15	CH_3	methyl radical	9.8380 ± 0.0004	[23]
16	CH_4	methane	12.618 ± 0.004	[24]
26	HC≡CH	acetylene	11.40081 ± 0.0001	[25]
27	CH_2=CH	vinyl radical	8.468 ± 0.029	[26]
28	CO	carbon monoxide	14.0136 ± 0.0005	[27]
29	HCO	formyl radical	8.15022 ± 0.00006	[28]
30	CH_2=O	formaldehyde	10.8850 ± 0.0002	[29]
55	CH=CH-CHO	formyl vinyl radical	8.51	†
55	O=C-CH=CH_2	acryloyl radical	6.93 (*trans*)	†
56	CH_2=CH-CHO	acrolein	10.11 ± 0.01	[30,31]
68	C_4H_4O	furan	8.88 ± 0.01	[32]
68	CH_2=CH-CH=C=O	vinylketene	8.29 ± 0.05	[33]
70	CH_3-CH=CH-CHO	crotonaldehyde	9.73 ± 0.01	[30,34]
70	CH_3-CO-CH=CH_2	methyl vinyl ketone	9.65 ± 0.02	[35]
70	CH_2=C(CH_3)-CHO	methacrolein	9.92 ± 0.05	[31]
83	O-C_4H_3O	2-furanyloxy radical	8.23	†
83	O=C=CH-CH-CHO	formyl ketenyl radical*	7.79 (*trans-cis*)	†
		(4-oxo-but-3-enal-2-yl)	7.66 (*cis-trans*)	†
			7.70 (*trans-trans*)	†
84	$C_4H_4O_2$	2(3H)-furanone‡	9.31	[36]
			9.67	[37]
84	$C_4H_4O_2$	2(5H)-furanone‡	10.22	[36]
			10.65 ± 0.1	[38]
96	C_4H_3O-CHO	furfural	9.22 ± 0.01	[39]
98	$C_5H_6O_2$	2-methoxyfuran	7.93 (*cis*)	†
		(2-MeOF)	7.79 (*trans*)	†
98	$C_5H_6O_2$	3-methyl-2(3H)-furanone‡	9.17	[36]
98	$C_5H_6O_2$	5-methyl-2(5H)-furanone‡	10.06	[36]
			10.12 ± 0.05	[40]
98	$C_5H_6O_2$	5-methyl-2(3H)-furanone‡	8.91	[36]
			8.97 ± 0.05	[41]

†average of CBS-QB3, G3 and CBS-APNO methods

*dihedrals O=C-C-C and CCCC

‡see Schemes 4 and 5 for structural information

profiles shown in Figure 1. The application Chemkin[43] was also used to simulate the reacting flow; details of these simulations are presented in the Kinetics section.

Results and Discussion

There are three main topics of methoxyfuran pyrolysis discussed here. First, is a description of the unimolecular reaction scheme and the primary products that account for the majority of observed decomposition. This is followed by an in-depth analysis of several observed bimolecular products; we postulate several routes to production of these species, including reactions with unreacted methoxyfuran or radical-radical reactions. Finally, the discussion concludes with a quantitative analysis of methoxyfuran consumption, including quantification of important intermediates, bimolecular routes and a comparison with kinetic mechanism predictions.

Unimolecular Decomposition Mechanism

The computational study of Simmie et al.[3] predicted that the dominant pathway for thermal decomposition of 2-methoxyfuran was loss of CH_3 to produce the allylic lactone 2-furanyloxy radical (m/z 83) as shown in Scheme 2. From here, the furanyloxy radical can ring open *via* a β-scission of the ring O1$-$C2 bond to a formyl ketenyl radical, 4-oxo-but-3-enal-2-yl, and eliminate CO to give a formyl vinyl radical, prop-1-ene-1-yl-3-one. The fate of the formyl vinyl radical,[44] likely not a stable intermediate in the microreactor, is decomposition to two molecules of CO, one H-atom, and one HC$\equiv$CH.

The unimolecular decomposition products of 2-methoxyfuran heated in helium and detected by 118.2 nm (10.487 eV) photoionization mass spectrometry (PIMS) are shown in Figure 2. With the SiC reactor held at 400 K, only the parent ion and the ^{13}C isotope are observed at m/z 98 and 99, respectively. Heating the reactor to 850 K triggers thermal decomposition and the observed ions are assigned as CH_3^+ (m/z 15), $C_2H_3^+$ (m/z 27), HCO^+ (m/z 29), $C_3H_3O^+$ (m/z 55), and 2-furanyloxy radical (m/z 83). As will be described shortly, only m/z 15 and 83 are assigned as

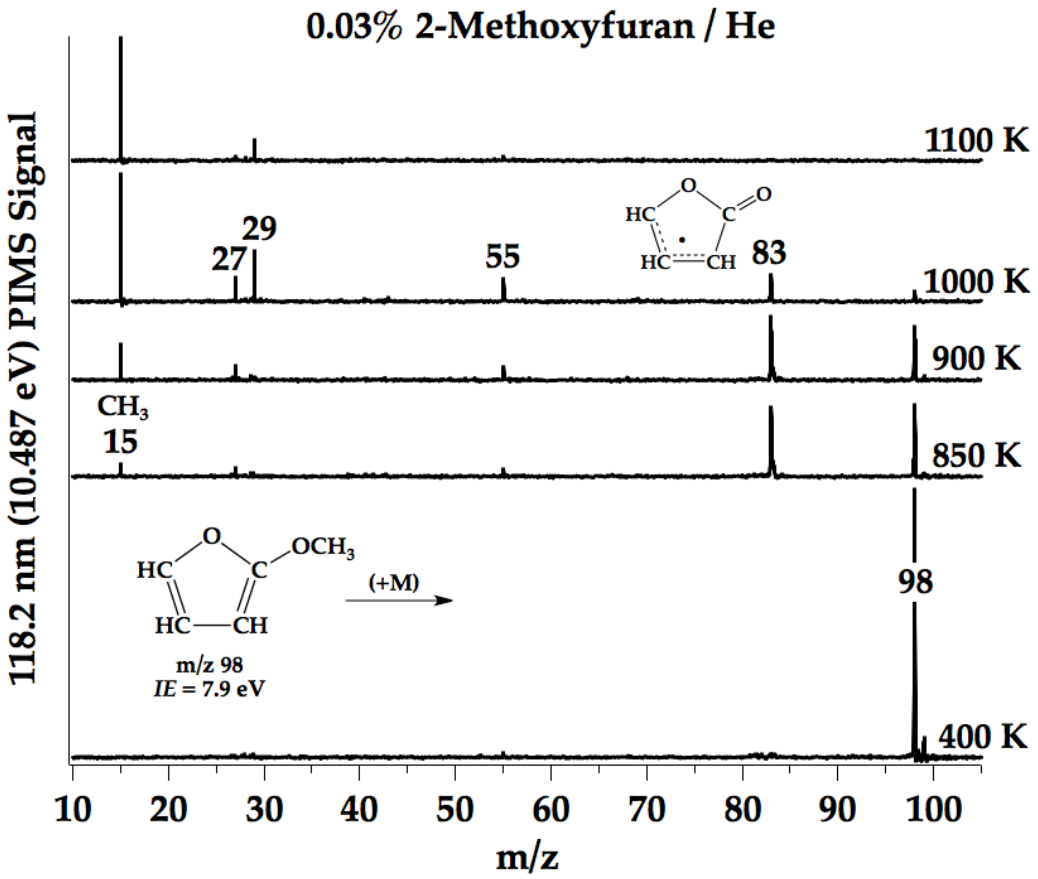

Figure 2: Mass spectra identify the unimolecular products from the pyrolysis of 2-methoxyfuran in helium in a pulsed flow heated SiC reactor. Products are ionized with 118.2 nm VUV photons (10.487 eV); temperatures indicated are the measured reactor wall temperature.

thermal products; the ions observed at 27, 29 and 55 are assigned to dissociative ionization[45] of either the parent or 2-furanyloxy. By 1100 K, all 2-methoxyfuran (m/z 98) is consumed.

Since the ionization energies of carbon monoxide[27] and acetylene[46] are beyond the range of the laser at 10.487 eV (see Table 1), the presence of acetylene from pyrolysis of a 0.04% mixture of 2-methoxyfuran in argon is demonstrated in Figure 3 by detection of the IR fundamentals ν_3(HC≡CH) at 3287 cm^{-1}, its associated Darling-Dennison resonance at 3301 cm^{-1}, and ν_5(HC≡CH) at 737 cm^{-1} in an Ar matrix.[47] Carbon monoxide as a thermal product can be difficult to detect because there is always a small background when the SiC reactor is heated (due to reaction with trace amounts of O_2), however the main absorptions at 2139 cm^{-1} and 2091 cm^{-1} for CO and ^{13}CO, respectively, are observed from pyrolysis of methoxyfuran.

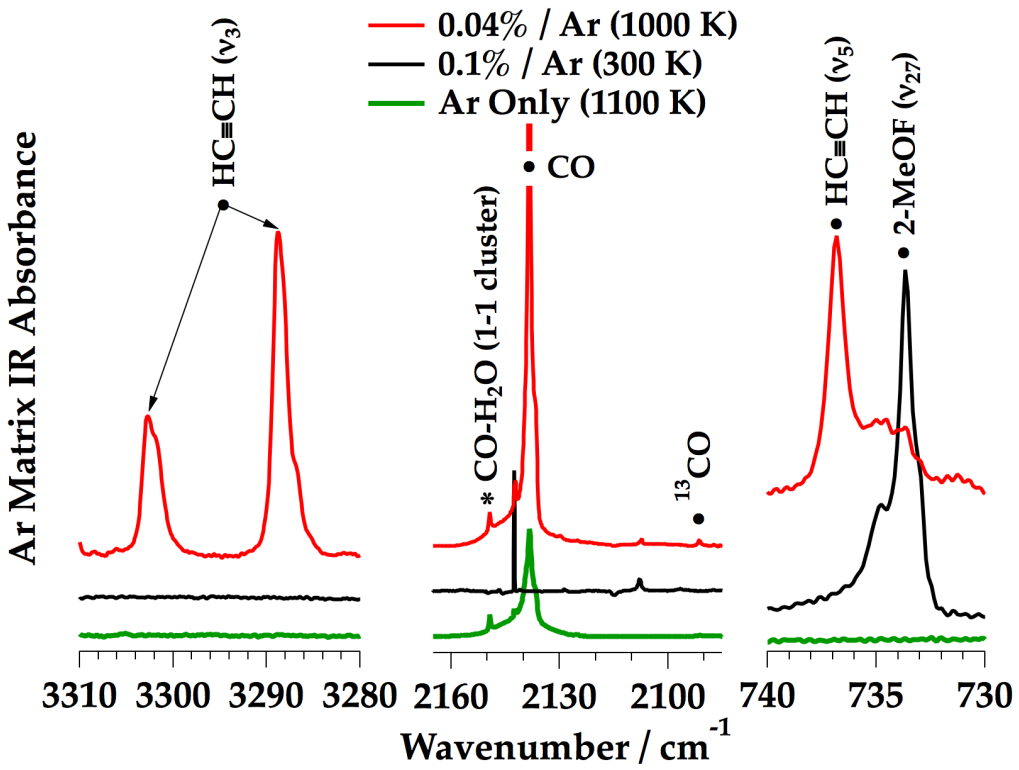

Figure 3: Infrared spectra identify acetylene (ν_3,ν_5) and carbon monoxide in Ar as a pyrolysis products of 2-methoxyfuran. Shown for comparison are reference scans with only argon passed through an 1100 K SiC reactor and the reactant mixture (2-MeOF) through an unheated reactor.

The mass spectra in Figure 4 show the major pyrolysis products from a 0.01% mixture of 2-methoxyfuran in helium through a continuous flow reactor at LBNL's Advanced Light Source (ALS). The left-hand panel of Figure 4 demonstrates that pyrolysis of 2-methoxyfuran at 950 K generates m/z 83 when 8.5 eV is used to photoionize. If the energy of the VUV is increased to 10.1 eV (right-hand panel), the CH_3 radical (m/z 15) is detected and new ions appear at m/z 29, 55, and 70 (the feature at m/z 58 is not a thermal product but instead is an acetone impurity due to an inadequate purge after cleaning between experiments at the ALS; 950 K spectrum sampled five times more spectra than 300 K, and thus m/z 58 is larger in the heated compared to the room temperature spectrum). We assign the ions HCO^+ (m/z 29) and $C_3H_3O^+$ (m/z 55) to dissociative ionization of either 2-furanyloxy radical (m/z 83) or a vibrationally excited methoxyfuran. None of these ions appear in the 10.1 eV PIMS of 2-methoxyfuran at 300 K and indeed, if they were thermal

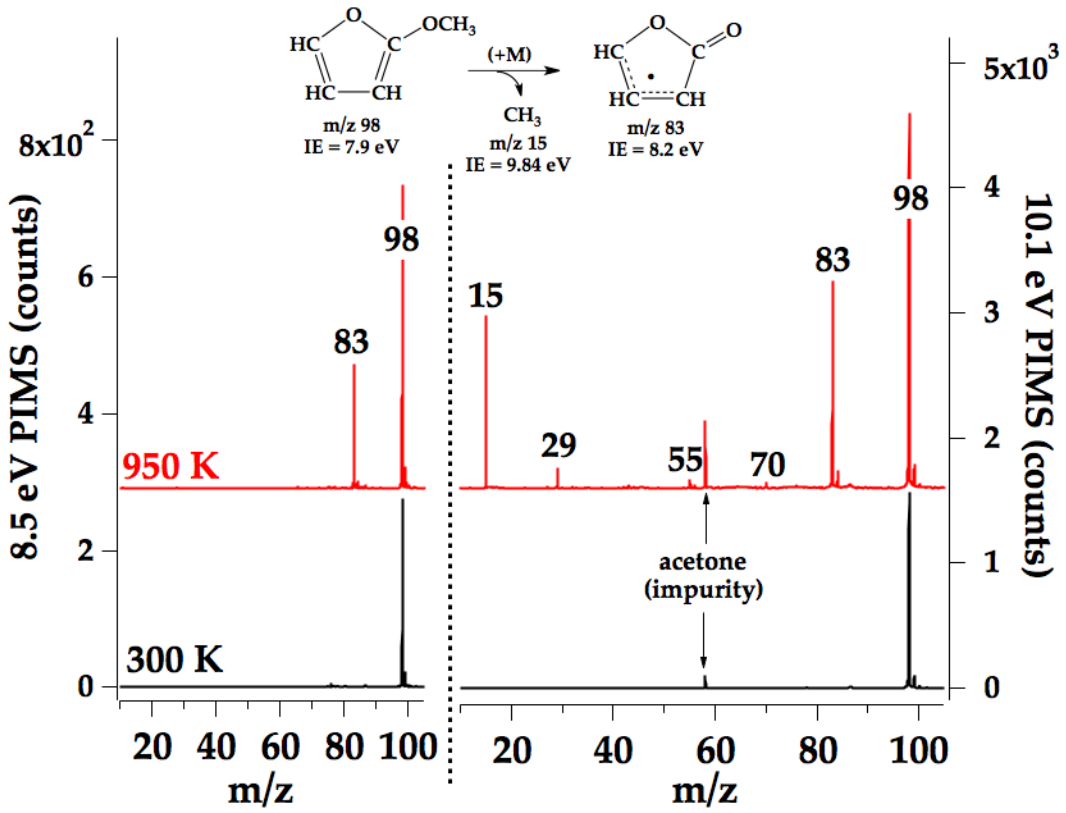

Figure 4: Dual photon energy mass spectra from pyrolysis of 0.01% methoxyfuran in He in a continuous flow reactor distinguish ions resulting from dissociative ionization from those formed thermally. Mass spectrum at 950 K sampled 500,000 individual mass spectra; 300 K sampled 100,000 mass spectra.

products, both m/z 29 and 55 should be observed in the PIMS at 8.5 eV. The species at m/z 70 is a secondary pyrolysis product of 2-methoxyfuran and arises from either radical addition reactions to the ring or CH_3 radical reactions with 2-furanyloxy radical, both possibilities are discussed in proceeding sections.

Figure 5 also includes a set of PIE curves that identify the primary unimolecular products from the thermal decomposition of 2-methoxyfuran as furanyloxy radical (m/z 83), CH_3 radical (m/z 15), and HC≡CH (m/z 26); ions from carbon monoxide (m/z 28) also appear at 14 eV but are not included in this plot. The measured photoionization cross-sections of methyl radical[48] and acetylene,[49] plotted as solid lines, are shown for comparison. The observed ionization thresholds of PIE(m/z 83) and PIE(m/z 98) are consistent with the calculated values of 8.2 eV and 7.8/7.9

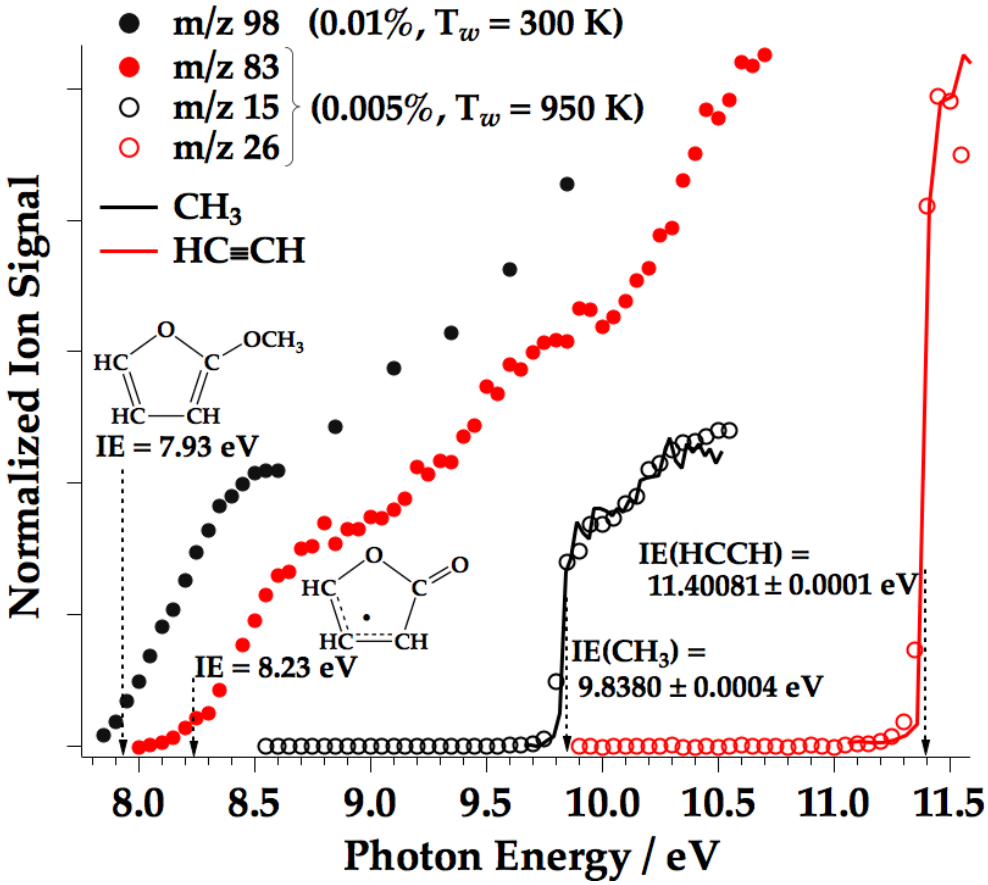

Figure 5: PIE curves and ionization energies of 2-methoxyfuran (m/z 98) and the primary unimolecular products 2-furanyloxy radical (m/z 83), methyl radical[23] (m/z 15) and acetylene[25] (m/z 26). Shown for comparison as solid lines are the photoionization cross-sections of methyl[48] and acetylene.[49]

eV for 2-furanyloxy radical and 2-methoxyfuran, respectively. The ion signal at m/z 83 begins to grow in at 8.1 eV, although 0.1 eV lower than predicted, it is about 0.4 eV above the predicted ionization threshold for any of the formyl ketenyl radical, O=C=CH-CH-CHO, conformations (see Table 1) suggesting that the lifetime of this intermediate is too short to be detected at the exit of the microreactor.

A set of photoionization efficiency curves at m/z 55 are shown in Figure 6. No ion signal at mass 55 is observed until above 10 eV at elevated temperatures, indicating the formyl vinyl radical in Scheme 2 (or acryloyl radical as in Table 1) is not a stable intermediate and its lifetime is too short to be detected under the conditions in the reactor. Based on the predicted ionization energies

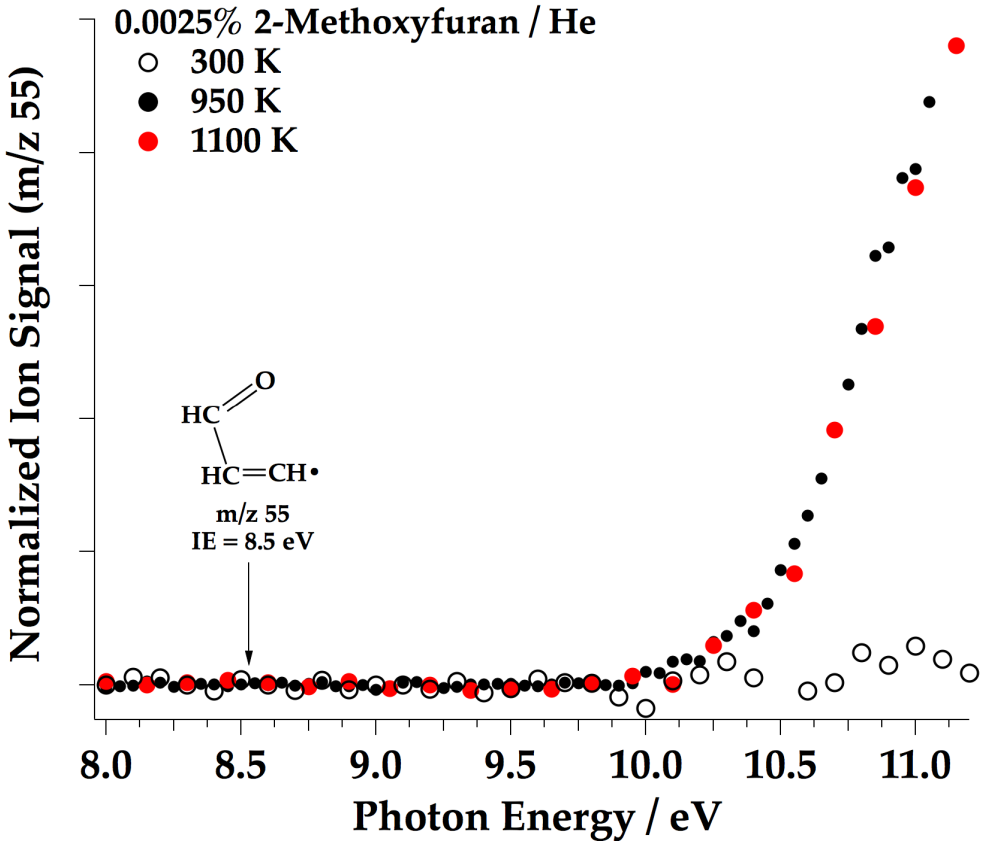

Figure 6: Photoionization efficiency curves of m/z 55 at several reactor temperatures. The lifetime of the proposed formyl vinyl radical intermediate is too short to be observed at the reactor exit; instead only signals due to dissociative ionization of other species are observed above 10 eV.

shown in Table 1, any species at m/z 55 should ionize well below 10 eV if formed as a stable thermal product.

The presence of the 2-furanyloxy radical as a stable intermediate was also identified by IR spectroscopy in an Ar matrix, as shown in Figure 7. From the electronic structure calculations, the intense feature at 1733 cm^{-1} is assigned as ν_4(C=O stretch of 2-furanyloxy radical). The location of the carbonyl stretch is consistent given the structure of this allylic lactone. The C−O bond in furanyloxy has been calculated to be shorter than a typical C−O single bond and closer to a typical C=O bond.[3,6] Other vibrational assignments in Figure 7 include ν_8, ν_{13}, and ν_{18}. There are also features at 1709 cm^{-1} and 1749 cm^{-1} (see Figure 10) that are also tentatively assigned to ν_4 of 2-furanyloxy. An IR study of 2(5H)-furanone in an Ar matrix[50] reports that the carbonyl

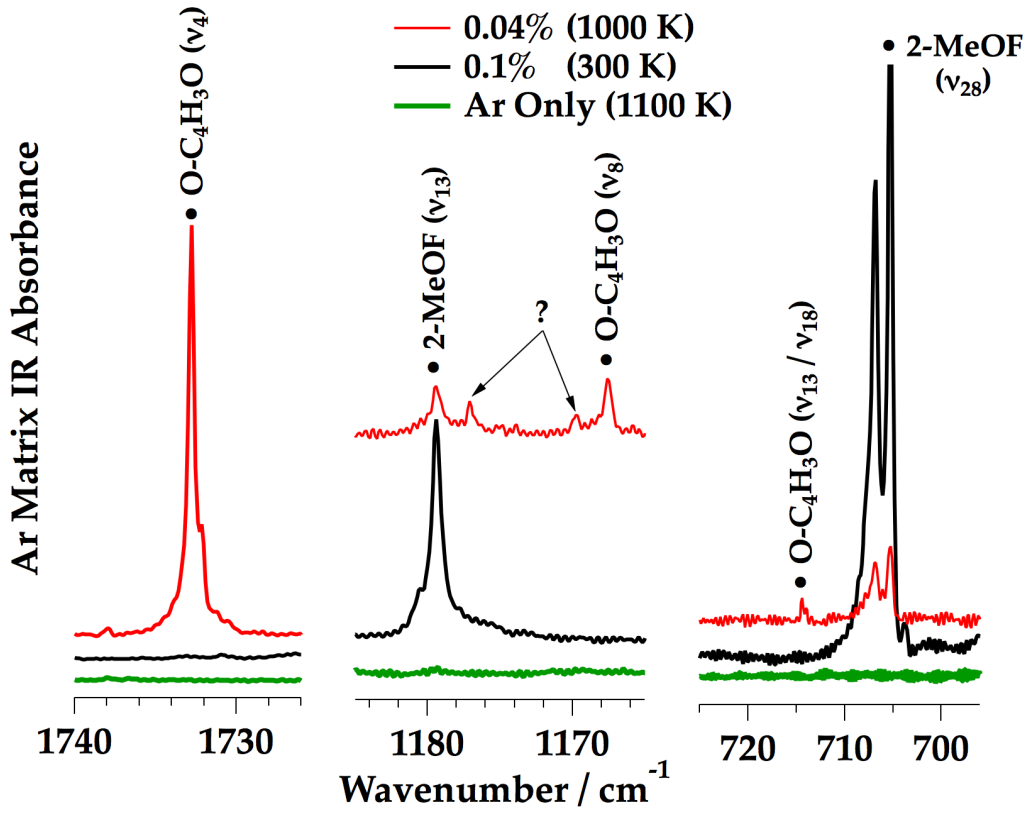

Figure 7: Select vibrational assignments of 2-furanyloxy (O-C_4H_3O) radical in an Ar matrix compared to scans of only Ar through a heated reactor and methoxyfuran (2-MeOF) in Ar through an unheated reactor. Features marked (?) are tentatively assigned to ν_8 of 2-furanyloxy.

stretch is very anharmonic, exhibiting several satellite peaks in the IR, possibly due to Fermi-resonance type bands. Since the furanyloxy radical has a very similar structure to 2(5H)-furanone (see structure in Scheme 3), it may behave similarly in an argon cage. The questionable features at 1170 cm^{-1} and 1177 cm^{-1} could also be satellite features of ν_8-furanyloxy or interaction bands in Ar. A tabulated summary of observed and calculated vibrational frequencies is included in the Supporting Information.

A careful search in the IR also shows no trace of the formyl ketenyl (O=C=CH-CH-CHO) or formyl vinyl (CH=CH-CHO) radicals in an Ar matrix, which, if present, should both have intense features due to the carbonyl stretch. This corroborates the findings of the PIE curves at m/z 55 and 83 (Figures 5 and 6), confirming these are not stable or detectable intermediates.

Bimolecular Reactions in Methoxyfuran Pyrolysis

Although the pyrolysis experiments presented here are performed at very dilute conditions, the potential for minor secondary products resulting from reactions of H atoms and CH_3 radicals with 2-methoxyfuran should also be considered. Scheme 2 predicts that for every molecule of 2-methoxyfuran that decomposes, one H-atom and one CH_3 radical are produced. Both of these radicals are very reactive and it is possible that they might abstract a hydrogen or add to the ring of unreacted methoxyfuran. In addition, the 2-furanyloxy radical (O-C_4H_3O) is also a persistent radical, and possible species resulting from bimolecular reactions of this species are also considered.

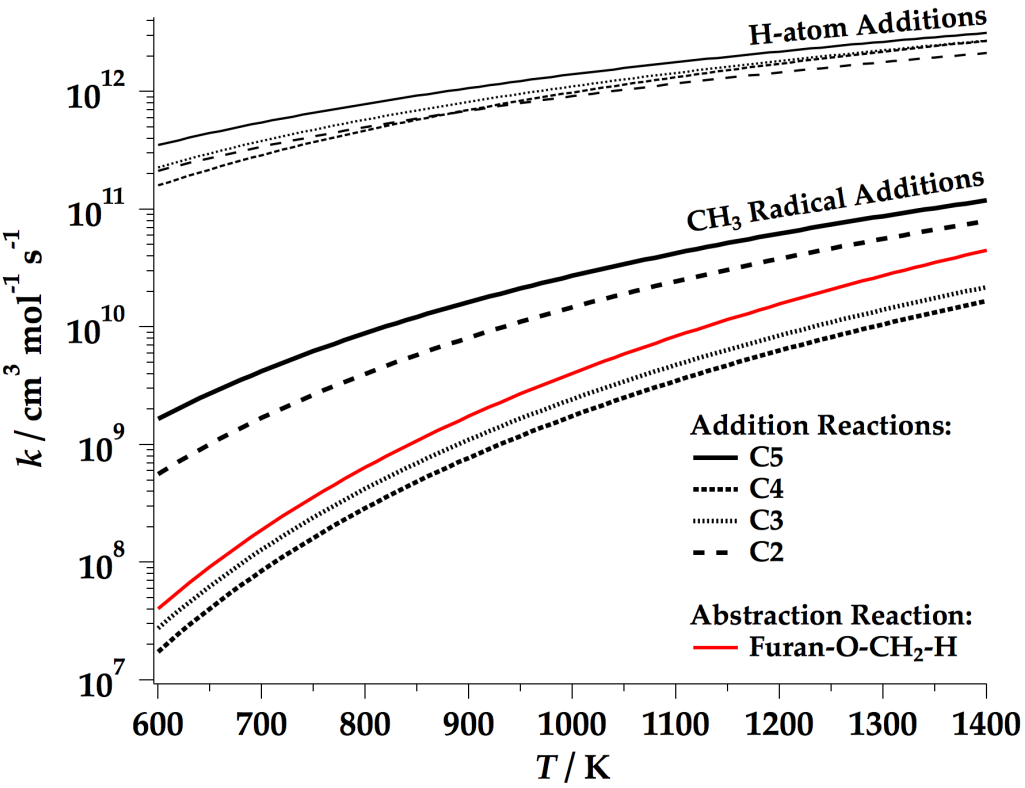

Figure 8: Calculated rate constants of H and CH_3 addition reactions to different positions on the methoxyfuran ring; also included is the hydrogen abstraction reaction by CH_3 at C7.

Calculated bimolecular rate constants for addition and abstraction reactions of methyl radical were included in the original quantum chemical study of methoxyfuran by Simmie et al.;[3] new to this study are addition reactions with hydrogen atom. The rate constants from 600−1400 K

of these possible routes are summarized in Figure 8 and have been used to speculate plausible bimolecular routes; a summary of the bimolecular rate constants are also included in Table 2. A few important aspects to note about these rate constants: at 1000 K H-atom addition reactions are two orders of magnitude faster than the fastest CH_3 addition reaction at C5 on the methoxyfuran ring (see Scheme 1 for ring position notations). Also, the rate constant for methyl addition at C3 or C4 is another order of magnitude lower than addition at C5.

In a related thermal decomposition study of furan (see Ref. 12), it was found that under similar operating conditions hydrogen-atom radical addition reactions could be avoided at a dilution of 0.01% furan in He. On the other hand, when thermally cracking methoxyfuran, H-atoms and CH_3 radicals were formed at lower temperatures and at faster time scales within the reactor, so it was found that a dilution of about 0.0025% methoxyfuran in He was required to ensure negligible secondary product formation in the continuous flow reactor. As discussed in Experimental Methods, the residence time in the reactor is essentially a fixed experimental parameter and decreasing the time spent in the reactor cannot necessarily be a viable option for reducing bimolecular reactions; instead this task is best accomplished through dilution.

In addition to the primary unimolecular products, there are several species that grow in as the reactant concentration is increased. Figure 9 is an expanded view of the mass spectra from Figure 4, including two more elevated temperatures. These spectra show that new ions at m/z 56, 68, 70 and 84 appear and persist even after all methoxyfuran has been consumed.

Addition Reactions of H and CH_3

An assortment of possible products resulting from H or CH_3 additions to unreacted methoxyfuran are shown in Schemes 3 and 4, respectively. In addition to the predicted rate constants of these reactions in Figure 8, the combination of infrared spectroscopy and photoionization efficiency curves aid in the identification of the relevant reaction channels.

Figure 10 compares the carbonyl region of the infrared spectrum of a dilute mixture (0.04%) of methoxyfuran in Ar, thin black line, to a more concentrated mixture (0.1%), red line. Products

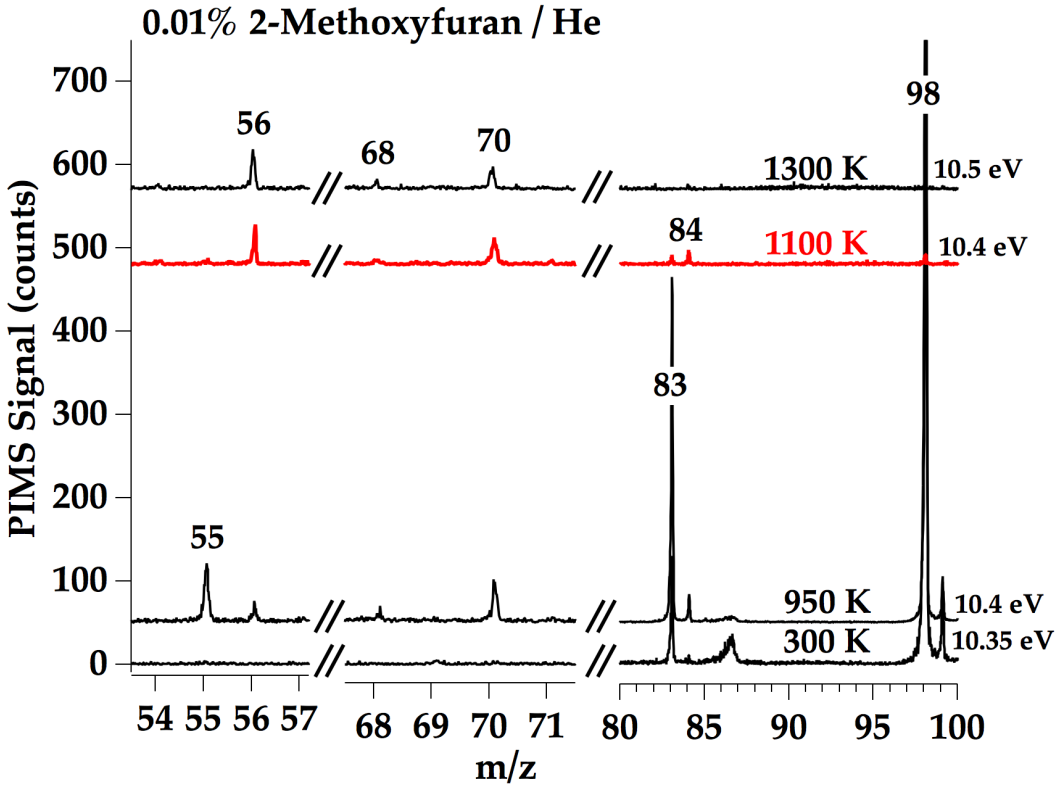

Figure 9: Thermal products at m/z 56, 68, 70 and 84 assigned to bimolecular chemistry. Dissociative ionization of 2-methoxyfuran to m/z 83 is observed at 300 K and 10.35 eV; the feature extending from m/z 86 to 88 is also the result of dissociative ionization and is an artifact of the reflectron time-of-flight operation.

detected from the 0.1% mixture at 1100 K include formaldehyde, methyl vinyl ketone (MVK or CH_3CO-$CH{=}CH_2$), and the unsaturated aldehydes acrolein ($CH_2{=}CH$-CHO) and crotonaldehyde ($CH_3CH{=}CH$-CHO), while only formaldehyde and acrolein are detected as secondary products from the dilute mixture at 1000 K. Figure 11 expands on the 1100 K spectrum in the region $1720-1695$ cm^{-1}, identifying MVK, acrolein and crotonaldehyde by comparison to authentic samples in an Ar matrix. The reactor was heated during part of the acrolein/Ar deposition in order to induce isomerization to the less thermodynamically stable *cis* conformation (similar to the approach used by Blom et al.[51]). The growth of split peaks at 1714 and 1715 cm^{-1} are assigned to *cis*-$CH_2{=}CH$-CHO,[52] while *trans*-$CH_2{=}CH$-CHO absorbs at 1708 cm^{-1}. The lone unlabeled feature in Figure 11 at 1709 cm^{-1} is likely the satellite peak of the furanyloxy radical (ν_4), as it

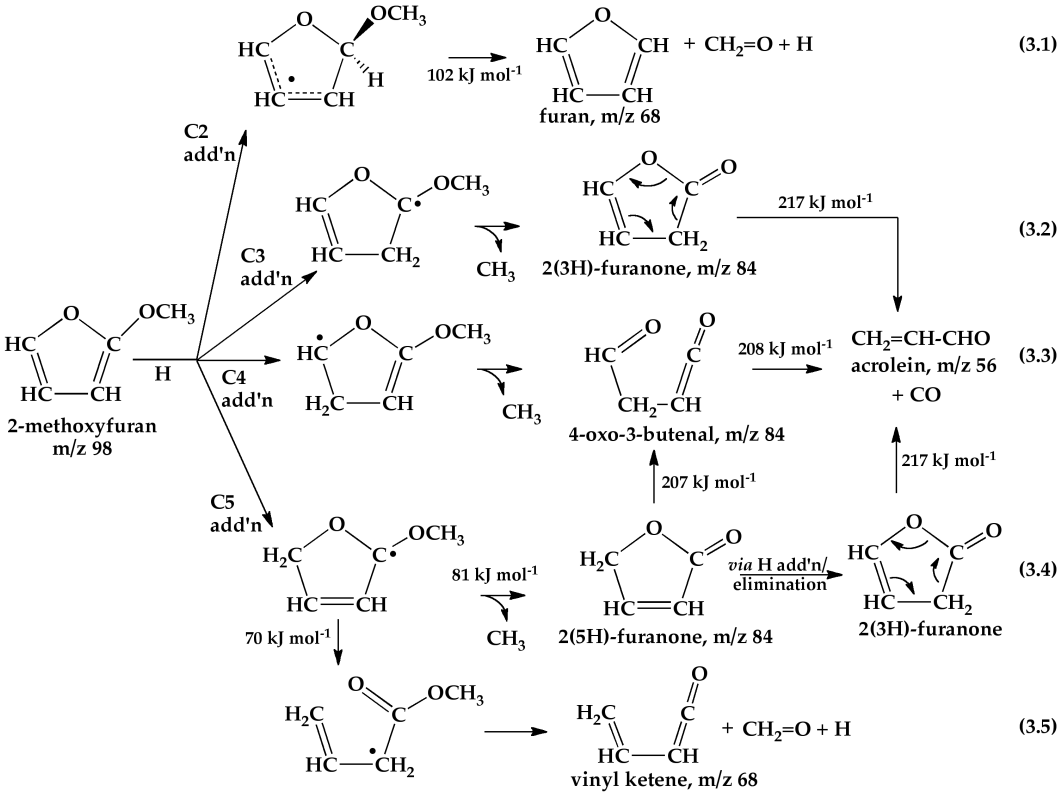

Scheme 3: Hydrogen-atom addition reactions to 2-methoxyfuran and possible resulting products. Calculated reaction barrier heights for select decomposition routes also indicated.

is present in both the dilute and concentrated product spectra. A tabulated summary of vibrational frequencies is presented in the Supporting Information.

When compared to the concentrated mixture in Figure 10, the only secondary product species detected from pyrolysis of the dilute mixture are CH_2=CH-CHO and CH_2=O. Both of these species can result from H-atom addition reactions to the ring, as shown in Scheme 3.1 and 3.5 for formaldehyde and Schemes 3.2 through 3.4 for acrolein. As shown in the PIMS spectra in Figure 9, a trace of m/z 68 is also observed. There are two possible identities for m/z 68: (1) an H-atom addition to C2 (Scheme 3.1) could eliminate methoxy radical and produce furan (C_4H_4O), or (2) the C5 radical addition intermediate could ring-open as in Scheme 3.5, and also eliminate methoxy radical resulting in vinylketene (CH_2=CH-CH=C=O). The ion signal grows in near the ionization threshold of furan (IE = 8.88 eV)[32] but the signal is barely above the noise level. Examination of the infrared spectra were also unable to provide additional confirmation of the identity of m/z 68,

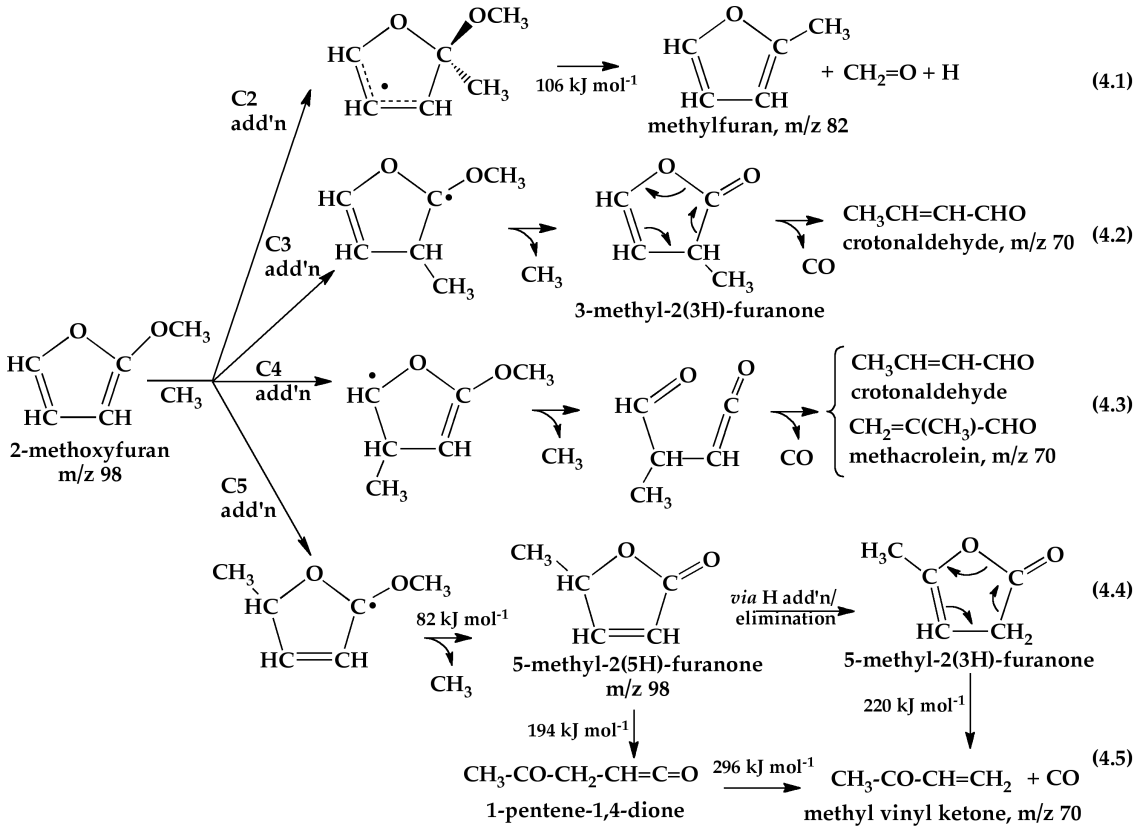

Scheme 4: Methyl radical addition reactions to 2-methoxyfuran and possible resulting products. Calculated reaction barrier heights for select decomposition routes also indicated.

indicting that it's formation by hydrogen atom addition reactions in Schemes 3.1 and 3.5 are less likely than formation of acrolein, which could result from H-addition at all other positions.

Photoionization efficiency scans further confirm the presence of acrolein and crotonaldehyde at 950 K, 1100 K, and 1300 K for different reactant mixture concentrations in a continuous flow of helium. The upper half of Figure 12 demonstrates that the ions at m/z 56 begin to grow in at 10.1 eV, the ionization threshold of acrolein[30,31] and the PIE(m/z 56) curve closely resembles the known photoionization cross-section for CH_2=CH-CHO.[53]

PIE curves of m/z 70, also in Figure 12, indicate the presence of crotonaldehyde as a dominant thermal product. The bottom half of Figure 12 shows the PIE(m/z 70) curves that result from pyrolysis of 2-methoxyfuran in helium through a reactor with continuous flow. The solid lines are the measured photoionization cross-sections of methyl vinyl ketone (CH_3-CO-CH=CH_2),

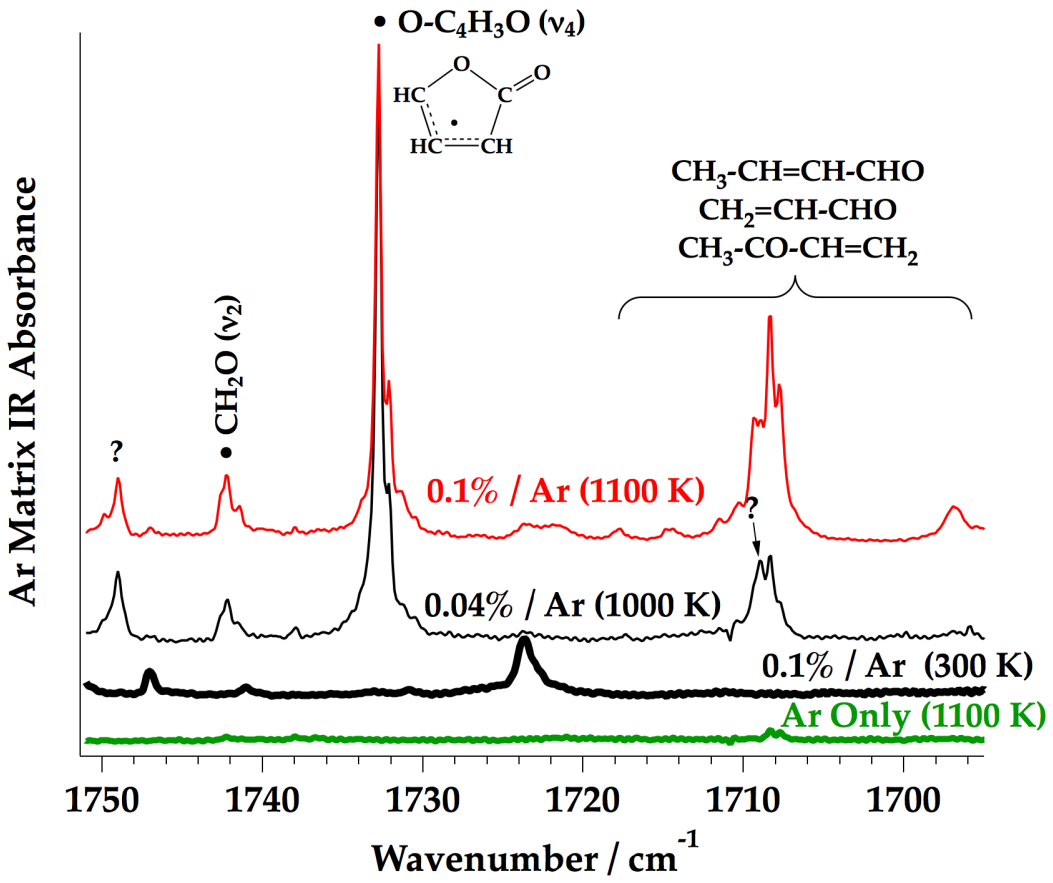

Figure 10: FT-IR product spectra compare the carbonyl region of a concentrated mixture (0.1%) of methoxyfuran in Ar to a dilute mixture (0.04%). Also included are scans of only Ar through a heated reactor and methoxyfuran in Ar through an unheated reactor. Uncertain bands (?) at 1749 and 1709 cm^{-1} tentatively assigned to ν_4 of 2-furanyloxy (O-C_4H_3O).

crotonaldehyde (CH_3-CH=CH-CHO) and methacrolein (CH_2=C(CH_3)-CHO), potential product species at m/z 70. Crotonaldehyde ionizes at 9.73 eV[30,34] and the IE(methyl vinyl ketone) and IE(methacrolein) are 9.65 eV[35] and 9.92 eV,[31] respectively. The PIE(m/z 70) trace rises at about 9.75 eV and follows the general trend of the crotonaldehyde curve; however, based on the shape of this curve we cannot rule out trace amounts of methyl vinyl ketone or methacrolein. Potential absorbance features in the infrared that could confirm the presence of methacrolein are obscured by the clearly more prominent products, acrolein and crotonaldehyde.

A scan of PIE(m/z 84) is unable to definitively identify which species in Scheme 3 are intermediates of hydrogen atom addition reactions due to interfering signals of the ^{13}C isotope from

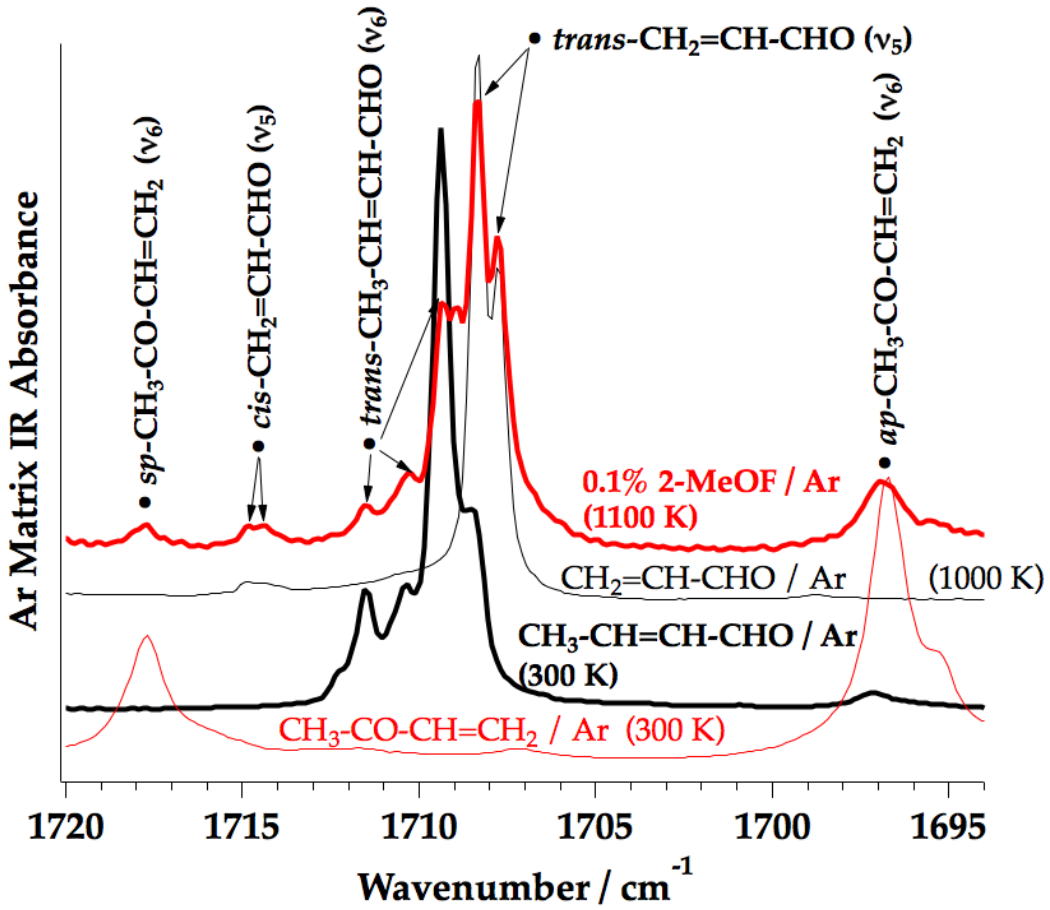

Figure 11: Authentic FT-IR spectra of acrolein, crotonaldehyde and methyl vinyl ketone in an Ar matrix, compared to product spectrum of a 0.1% mixture of methoxyfuran in argon heated to 1100 K (6.4 mmol deposited). Each authentic spectrum scaled relative to product spectrum as indicated; molecule(%-mixture/Ar, mmol Ar deposited, scaling factor): CH_3-CO-CH=CH_2 (0.09%, 6.4, 1:30); CH_3-CH=CH-CHO (0.06%, 4.0, 1:13); CH_2=CH-CHO (0.05%, 5.8, 1:13).

mass 83. Examination of PIE(m/z 84) at 1300 K when all m/z 83 is consumed does show that trace amounts of m/z 84 grow in between 9.5−10 eV, which could indicate the possibility of both 2(3H)-furanone (IE = 9.3−9.7 eV) and 2(5H)-furanone (IE = 10.2−10.65 eV).[36,37] The ionization energy[37] of 2(5H)-furanone is likely lower than the reported value of 10.65 eV; samples of 2(5H)-furanone seeded in He were pulsed through an unheated reactor and ions at m/z 84 were detected by 10.487 eV photoionization mass spectrometry. A more detailed discussion of these experiments is reported elsewhere;[56] a quantum chemical study of the thermochemistry and kinetics of these lactones is also presented in works by Würmel and Simmie.[36,57]

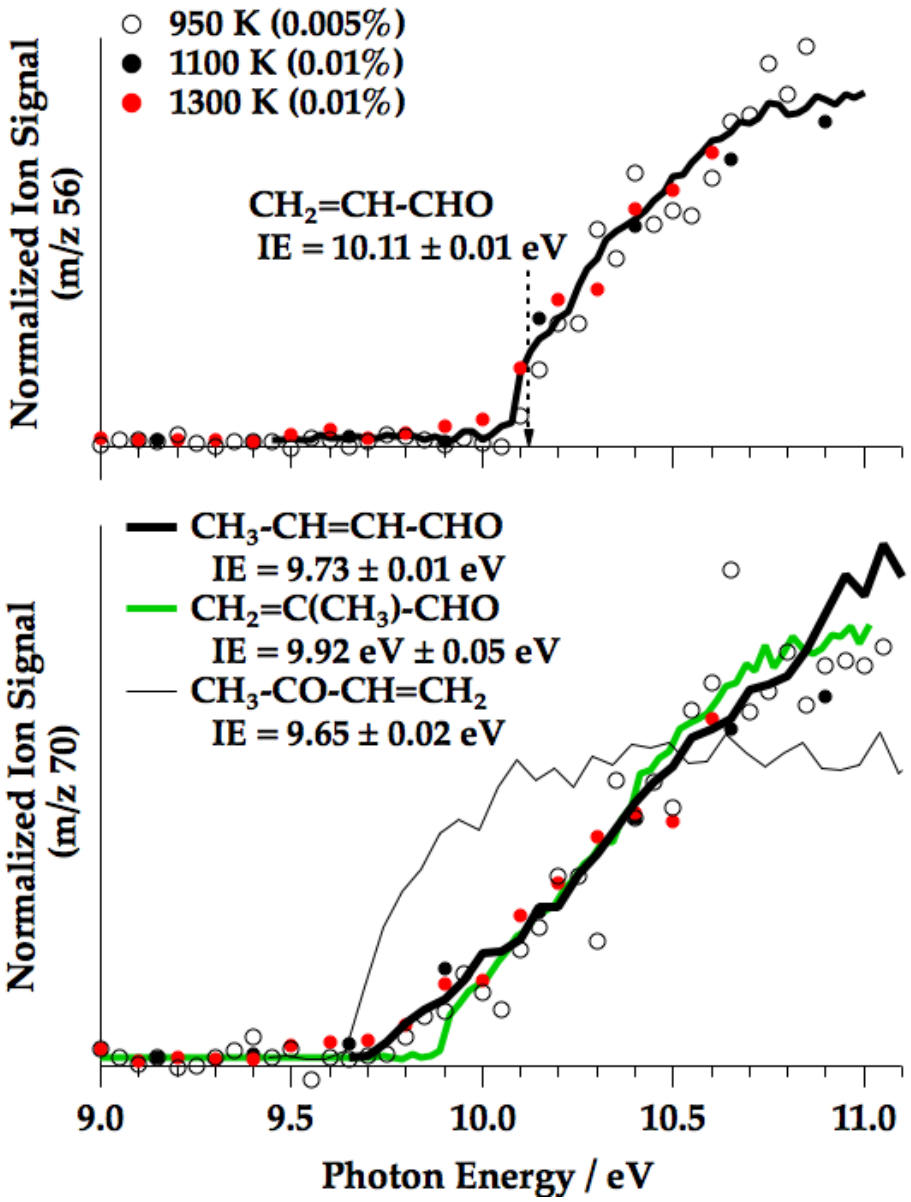

Figure 12: Photoionization efficiency curves of m/z 56 and m/z 70 recorded at three reactor temperatures. The photoionization cross-sections and ionization energies of CH_2=CH-CHO,[30,31,53] CH_3-CH=CH-CHO,[30,34,54] CH_3-CO-CH=CH_2 [35,54] and CH_2=C(CH_3)-CHO[31,55] are included.

Examination of the PIE(m/z 98) in Figure 13, on the other hand, provides insight into which intermediate species in Scheme 4 is formed in the microreactor. Samples of 2-methoxyfuran at 300 K and 950 K in a continuous flow helium reactor show an appearance energy of 7.9 eV which is compatible with the calculated IE(2-methoxyfuran). Heating a very dilute sample (0.0025%) of 2-methoxyfuran to 1100 K produces no ions at m/z 98, indicating all methoxyfuran is consumed and

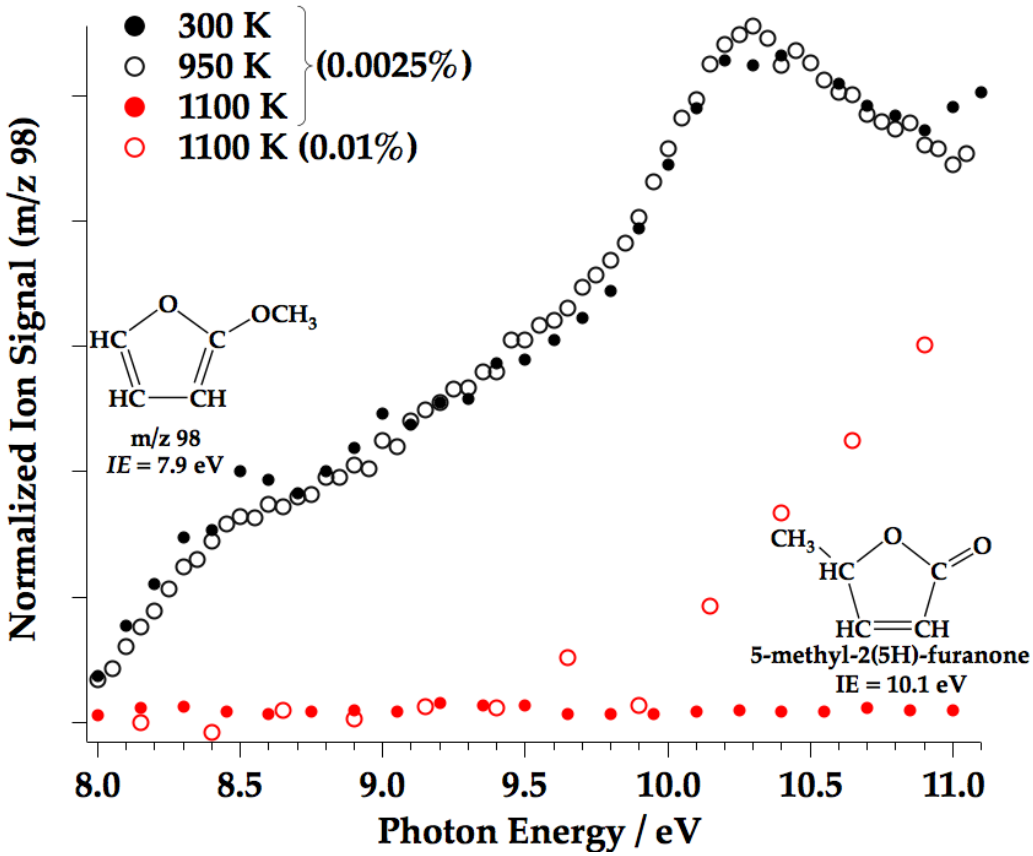

Figure 13: Photoionization efficiency curves of m/z 98. Mass 98 that appears at 1100 K from pyrolysis of a 0.01% mixture could be 5-methyl-2(5H)-furanone from CH_3 addition at C5 on 2-methoxyfuran (see Scheme 4).

no species associated with bimolecular reactions are observed. When a more concentrated mixture (0.01%) is heated to 1100 K, an ion signal at m/z 98 appears well above 7.9 eV. The CH_3 radical addition reactions in Scheme 4 could lead to an intermediate at m/z 98 and based on estimates of the ionization energies of these intermediate species, shown in Table 1, 5-methyl-2(5H)-furanone, formed by addition of CH_3 at C5 on methoxyfuran, has an ionization threshold just above 10 eV.[36] If the intermediate was the result of CH_3 addition at C3, as in Scheme 4.2, the predicted ionization threshold for this methylated 2(3H)-furanone is 1 eV lower in energy.

The methyl vinyl ketone that appears in trace amounts in the IR spectrum of Figure 11 is likely due to decomposition of the methylated 5-methyl-2(5H)-furanone. There are a few possible decomposition routes for this species that could result in the formation of methyl vinyl ketone.

Recent electronic structure calculations indicate[57] that the lowest-energy decomposition route of 5-methyl-2(5H)-furanone is ring opening to 1-pentene-1,4-dione, as shown in Scheme 4.5. The furanone could also decompose through an addition-elimination reaction with H-atom, converting the 2(5H) intermediate to 5-methyl-2(3H)-furanone (α-angelica lactone), which has been shown to eliminate CO and produce MVK either through a concerted reaction[56,58] or through an open-chain pentene-dione intermediate.[57] A similar addition-elimination reaction was suggested[36] to be a favorable route to interconvert the un-methylated furanones, 2(3H)- and 2(5H)-furanone. A more complete account on the experimentally measured decomposition patterns of the furanones and methylated furanones is reported elsewhere.[56]

Finally, the absence of PIMS signals at m/z 82 excludes CH_3 addition to 2-methoxyfuran at the C2 position. Indeed the rate constant for this reaction at 1000 K is two times slower than methyl addition at C5. Exclusion of reaction at the C2 position therefore excludes reactions at C3 or C4 as they are predicted to be another order of magnitude slower.

Reactions with 2-Furanyloxy Radical

Both the PIE(m/z 83) and the vibrational signatures in the IR demonstrate that 2-furanyloxy radical (m/z 83) is a persistent radical. Consequently, products resulting from reactions of H-atoms or CH_3 radicals with this species must also be considered. Several possible chemical outcomes of these reactions are shown in Scheme 5.

Concerted elimination of 3-methyl-2(3H)-furanone to crotonaldehyde and CO, shown in Scheme 5.1, is a likely decomposition route. Scheme 4 also predicts formation of crotonaldehyde by CH_3 addition at C3 or C4 on 2-methoxyfuran; however, the calculated rate constants in Figure 8 indicate CH_3 addition at C3 of methoxyfuran is slower than addition at C2; since no methylfuran at m/z 82 is observed in Figure 9 resulting from a C2 addition, we conclude reactions slower than this can be excluded. Therefore it is likely CH_3 radical reactions with 2-furanyloxy in Scheme 5.1 are the source of crotonaldehyde observed in both the infrared (Figure 11) and photoionization efficiency of m/z 70 (bottom half of Figure 12).

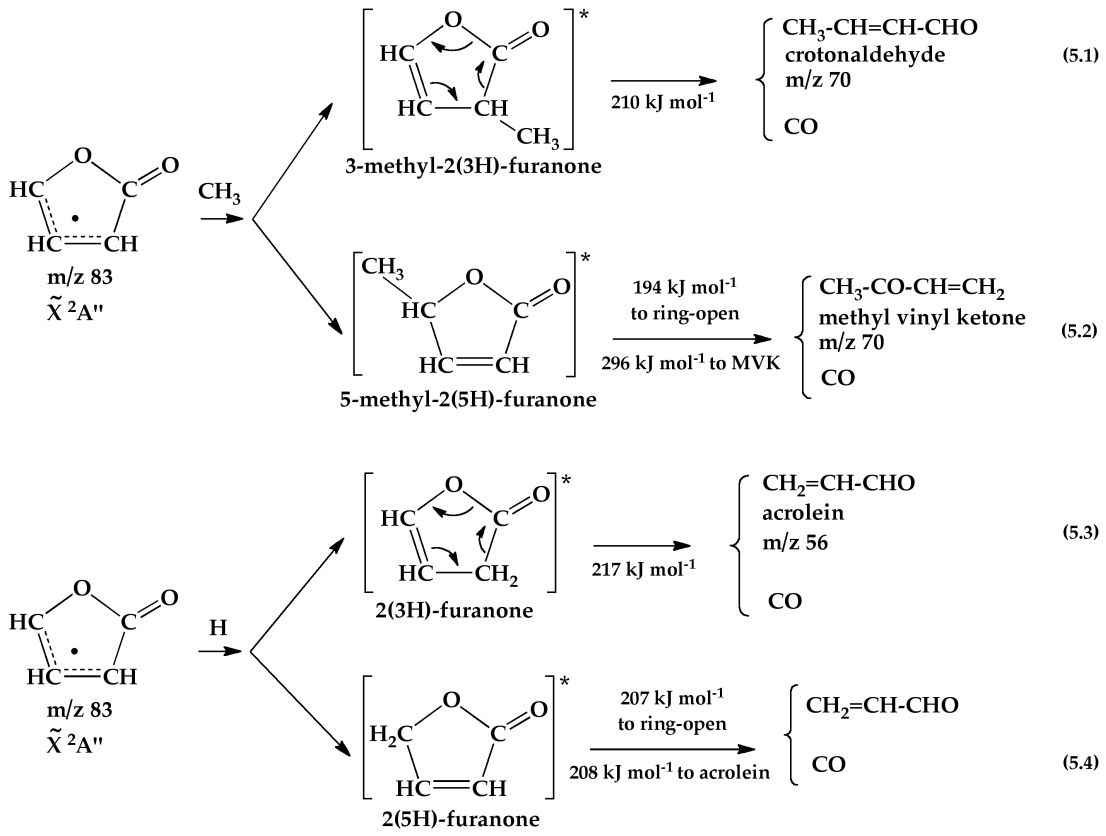

Scheme 5: Possible products resulting from reaction of H and CH_3 with 2-furanyloxy radical, including calculated reaction barriers.[36] Refer to Scheme 4.5 and Scheme 3.4 for structure of ring-opened intermediates (see Refs. 36, 57, 58 and 56 for more detailed theoretical predictions and experimental observations of several lactones).

Abstraction Reactions

The most favorable position for hydrogen atom abstraction by methyl or H-atom is from the methyl substituent group (on C7 as shown in Scheme 1), where the kinetics of H-atom abstraction by methyl is over an order of magnitude more favorable than at any ring hydrogen.[3] Upon abstraction, Scheme 6 suggests that the resultant aryloxy(methyl) radical,[5,59] m/z 97, can isomerize *via* a Mulcahy rearrangement[60,61] to furfural, m/z 96. PIMS spectra in Figure 9 shows no signals at m/z 96 or 97 for methoxyfuran diluted in He.

Based on the minimal evidence for furfural we conclude that abstraction reactions are unlikely under the operating conditions in the microreactor. Calculated rates of hydrogen abstraction by methyl are consistent with these results indicating that abstraction reactions only become compet-

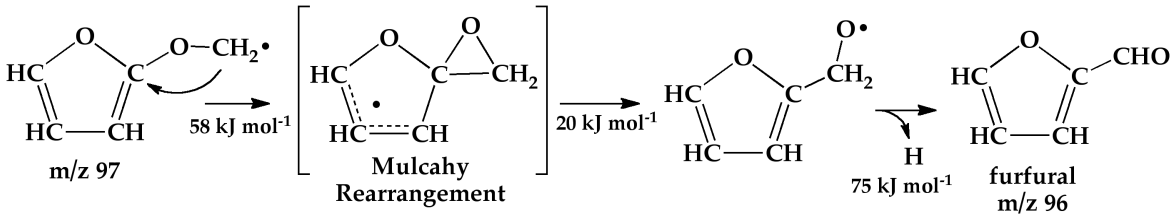

Scheme 6: Abstraction reaction scheme and calculated reaction barriers.

itive with CH_3 addition reactions at much higher temperatures[3] than those reported here.

Kinetics of Methoxyfuran Decomposition

Kinetic Mechanism

The simple methoxyfuran mechanism developed by Simmie et al.[3] is expanded upon in this work to include pressure-dependent reaction rates for the first two decomposition steps, thermodynamic parameters for individual species, in addition to rate constants for bimolecular reactions involving the parent and reactions of 2-furanyloxy radical with methyl radical and hydrogen atom. Rice-Ramsperger-Kassel-Marcus theory and Master Equation (RRKM/ME) analyses[62] of the thermally activated unimolecular reactions 1 and 2, shown in Table 2, were carried out using the ChemRate application.[63] The parameters for the computation of pressure dependence were chosen in accordance to those outlined in previous work of a not dissimilar system.[64] The updated mechanism, shown in Table 2, includes 27 species and 24 reactions. The notations for addition reactions are the intermediates formed when CH_3 or H adds to the methoxyfuran ring at the specified position (*i.e.* CH_3-C5 is the intermediate formed when CH_3 adds to methoxyfuran at the C5 position). At this time, no rate constants for the conversion of these bimolecular intermediates to final products are included in the mechanism. Thermodynamic parameters for species unique to methoxyfuran were calculated for the present work and the remainder were compiled from several kinetic mechanisms.[65,66] The reactor was simulated as a plug flow reactor using the calculated temperature and pressure conditions in Figure 1.

Table 2: Reaction mechanism with rate constant parameters. Notations for CH_3 or H addition reactions are the intermediates formed when CH_3 or H adds to the methoxyfuran (2-MeOF) ring at the specified position.

#	Reaction	A	n	E_a	Ref.
	Unimolecular Reactions				
1	2-MeOF $\rightleftharpoons$ O-C_4H_3O + CH_3 (k_∞)	9.32 x 10^{13}	0.00	184	
	(P = 100 atm)	8.55 x 10^{13}	0.00	189	
	(P = 1 atm)	6.42 x 10^{13}	0.00	187	
	(P = 0.01 atm)	7.90 x 10^{63}	-15.3	276	
	(P = 0.0001 atm)	9.38 x 10^{82}	-21.8	291	
2	O-C_4H_3O $\rightleftharpoons$ O=C=CH-CH-CHO (k_∞)	2.15 x 10^{15}	0.00	161	
	(P = 100 atm)	8.04 x 10^{36}	-6.623	196	
	(P = 1 atm)	2.81 x 10^{41}	-8.476	191	
	(P = 0.001 atm)	8.95 x 10^{39}	-9.017	172	
3	O=C=CH-CH-CHO $\rightleftharpoons$ CO + CH=CH-CHO	2.29 x 10^{15}	0.00	137	
4	CH=CH-CHO $\rightleftharpoons$ HCO + HC$\equiv$CH	1.01 x 10^{13}	0.00	121	
5	CH=CH-CHO $\rightleftharpoons$ O=C-CH=CH_2	4.56 x 10^{8}	0.00	94.4	
6	O=C-CH=CH_2 $\rightleftharpoons$ CO + CH_2=CH	3.19 x 10^{15}	0.00	108	
7	HCO $\rightleftharpoons$ H + CO	3.61 x 10^{13}	0.00	64.2	[67]
8	CH_2=CH (+M) $\rightleftharpoons$ H + HC$\equiv$CH (+M)	2.00 x 10^{14}	0.00	166	[68]
	CH_3 and H Addition/Abstraction Reactions				
9	CH_3 + 2-MeOF $\rightleftharpoons$ CH_4 + $C_5H_5O_2$	2.80 x 10^{0}	3.65	34.2	
10	CH_3 + 2-MeOF $\rightleftharpoons$ CH_3-C2	1.15 x 10^{4}	2.47	24.9	
11	CH_3 + 2-MeOF$\rightleftharpoons$ CH_3-C3	4.06 x 10^{4}	2.31	41.2	
12	CH_3 + 2-MeOF $\rightleftharpoons$ CH_3-C4	3.04 x 10^{4}	2.33	42.7	
13	CH_3 + 2-MeOF $\rightleftharpoons$ CH_3-C5	3.38 x 10^{4}	2.32	20.2	
14	H + 2-MeOF $\rightleftharpoons$ H-C2	3.55 x 10^{6}	1.908	5.99	
15	H + 2-MeOF $\rightleftharpoons$ H-C3	8.55 x 10^{6}	1.844	8.01	
16	H + 2-MeOF $\rightleftharpoons$ H-C4	4.92 x 10^{6}	1.947	10.3	
17	H + 2-MeOF $\rightleftharpoons$ H-C5	7.18 x 10^{6}	1.858	5.41	
	Radical-Radical Reactions				
18	O-C_4H_3O + CH_3 $\rightleftharpoons$ 3-CH_3-2(3H)Furanone*	1.64 x 10^{13}	-0.32	-0.55	
19	O-C_4H_3O + CH_3 $\rightleftharpoons$ 5-CH_3-2(5H)Furanone*	1.64 x 10^{13}	-0.32	-0.55	
20	O-C_4H_3O+ H $\rightleftharpoons$ 2(5H)-Furanone*	1.59 x 10^{14}	0.18	-0.52	
21	O-C_4H_3O + H $\rightleftharpoons$ 2(3H)-Furanone*	1.59 x 10^{14}	0.18	-0.52	
22	HCO + H $\rightleftharpoons$ H_2 + CO	9.00 x 10^{13}	0.00	0.0	
23	HCO + CH_3 $\rightleftharpoons$ CH_4 + CO	1.20 x 10^{14}	0.0	0.0	[66]
24	CH_2=CH + H $\rightleftharpoons$ HC$\equiv$CH + H_2	1.20 x 10^{13}	0.0	0.0	[66]

Units: cm^3 mol s kJ K; $k = AT^n \exp(-E_a/RT)$

*Recombination rate constants

A fully reactive CFD simulation was also performed,[9] utilizing a simplified mechanism with only the unimolecular reactions $1-4$ and 7 to model the conversion as a function of reactor temperature. For these simulations transport properties were required; available transport properties were taken from the Liu et al. furan mechanism[69] while the remainder were estimated.[70] Refer to the Supporting Information for the complete kinetic mechanism.

Consumption of 2-Methoxyfuran

Similar to the conversion measurements of Bruinsma et al.,[2] the conversion of 2-methoxyfuran in a continuous flow of He at several reactor wall temperatures and reactant concentrations was measured and is summarized in Figure 14. The experimental results are also compared to predictions using the kinetic mechanism in Table 2.

The extent of methoxyfuran consumption was determined by comparison of the photoion signal at four reactor wall temperatures to the observed ion signal in a room temperature scan of the same mixture. The vertical uncertainty limits applied to the experimental measurements were determined from the 2σ standard deviation of a PIE scan at m/z 98 collected at 950 K from 8.0 to 9.0 eV, averaging the observed conversion from 11 measurements. The uncertainty can in part be attributed to fluctuations of the reactor temperature throughout the length of the scan, approximately 10 minutes. The horizontal uncertainty limits of $\pm$ 30 K include an estimated uncertainty of the temperature measurement due to the thermocouple reading in addition to any potential drift of the temperature throughout a given measurement due to manual temperature control. In addition, temperature measurement with a 0.01 in diameter Type K thermocouple was used for these measurements in place of the standard 0.005 in diameter Type C thermocouple. Use of the larger diameter wire likely reduced the amount of contact between the thermocouple junction and the reactor wall, resulting in a less reliable temperature measurement.

The red lines in Figure 14 are the predicted conversion based on simulating the microreactor as plug flow in Chemkin,[43] with a constant mass flow rate of 280 sccm He and an initial concentration of 0.005% methoxyfuran. The gas temperature and pressure profiles along the length of the reactor

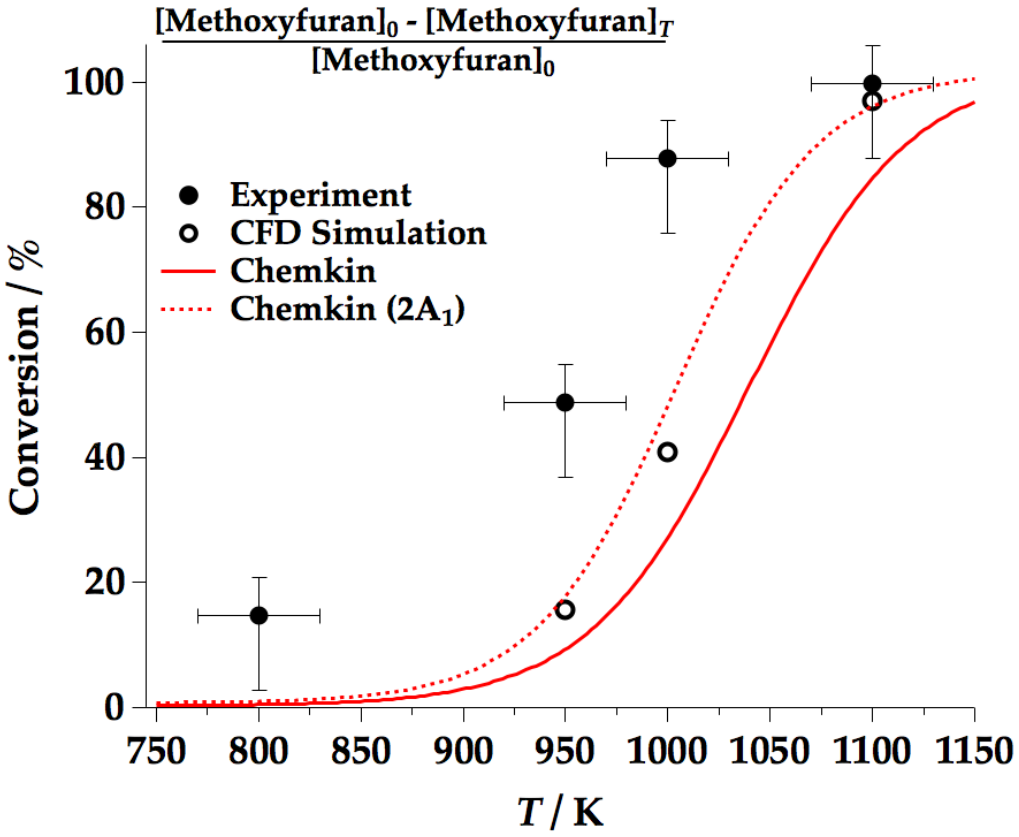

Figure 14: Measured percent conversion of 2-methoxyfuran as a function of external reactor wall temperature compared to predictions of reactive CFD simulations and Chemkin plug flow reactor simulations. Chemkin ($2A_1$) refers to a doubling of the A-factor of Reaction 1 in Table 2.

were determined by CFD. The %-conversion plotted in Figure 14 is average based on centerline temperature and the temperature a distance half way between centerline and the reactor wall. It was found that doubling the reactant concentration to 0.01% increases the conversion at a given temperature by approximately one percent. The dashed red lines are the result of doubling the A-factor for all pressure-dependent terms of Reaction 1 in Table 2, while the solid lines uses the rate parameters as written. In addition, a fully reactive CFD simulation was performed which included only limited reactions (1−4 and 7 in Table 2, all k_∞) to ensure a converged solution; these results are plotted as open circles.

As shown in Figure 14 most experimental data points follow the same s-shaped curve as the predictions but in general are larger. One major issue that needs to be addressed with this type

of measurement is accurately quantifying the ion signal when comparing over a range of temperatures. As the temperature of the fluid increases both the radial and axial velocity components of the molecular beam also increase. It is possible that some signal is lost due to a higher radial velocity component at elevated temperatures, and therefore the conversion would be overestimated when compared to the ion signal of a room temperature scan. Preliminary measurement on this effect are discussed in Ref. 56, indicating that a careful calibration or use of an appropriate internal standard is required for measurements of this sort in the future.

Quantification of 2-Furanyloxy Radical and Bimolecular Products

As shown in Scheme 2 the thermal decomposition of 2-methoxyfuran is initiated by cleavage of the $O-CH_3$ bond to form CH_3 and 2-furanyloxy radicals. Evidence in the IR and PIE(m/z 83) demonstrates the lifetime of 2-furanyloxy is long enough to survive the hot reactor and therefore it is valuable to quantify the amount of this unreacted radical present at a given temperature; this information is also useful to interpret the likelihood of radical-radical reactions.

With little experimental evidence for the formyl ketenyl (O=C=CH-CH-CHO) and formyl vinyl (CH=CH-CHO) radicals, here we assume all 2-furanyloxy decomposes to form the stable products CO, HCCH and H-atom. One way to quantify the radical pool of 2-furanyloxy is then to measure the loss of methoxyfuran compared to a room temperature scan while also monitoring the formation of the closed-shell products (HCCH or CO):

$$[\text{2-furanyloxy}] = [\text{2-methoxyfuran}]_{300\text{K}} - [\text{2-methoxyfuran}]_T - [\text{HCCH or CO}]_T \qquad (2)$$

Since it is difficult to measure the absolute concentration of a species, as described in detail in Ref. 12, use of Eq. (2) to estimate the concentration 2-furanyloxy is not desirable. Instead, a more straightforward approach is to compute the number density ratio of two molecular species using a formulation of the Beer-Lambert law for photoionization. This method was previously implemented in the measurement of product ratios for the thermal decomposition of furan[12] and the

metastable cyclopentadienone.[71] A similar method can be applied to methoxyfuran decomposition in an effort to quantify how much of the furanyloxy radical intermediate is present at a given temperature. Since the photoionization cross-section of this radical has not yet been measured, quantifying the observed ion signal must be accomplished in an indirect manner; one method is to measure the ratio of HCCH to CH_3:

$$\frac{[\text{2-furanyloxy}]}{[\text{CH}_3]} = 1 - \frac{[\text{HCCH}]}{[\text{CH}_3]} \tag{3}$$

and then assume, with some obvious uncertainty due to possible bimolecular reactions, that the remaining fraction is in the form of 2-furanyloxy. In order to cancel the photon-flux term, both measurements were made at the same photon energy, to estimate the ratio of acetylene to methyl radical:

$$\frac{[\text{HCCH}]}{[\text{CH}_3]} = \frac{S_{26}^{+}}{S_{15}^{+}} \frac{\sqrt{15}}{\sqrt{26}} \frac{\sigma_{\text{CH}_3}(\text{E})}{\sigma_{\text{HCCH}}(\text{E})} \tag{4}$$

where σ_i(E) is the reported photoionization cross-section, S_i^+ is the observed ion signal at a given photon energy and $\sqrt{m_i}$ is the mass discrimination factor. The resulting measured ratio of HCCH to CH_3 for a 0.005% mixture of methoxyfuran in helium at 950 K is 0.88 ± 0.27 and is summarized in Table 3. At 11.0 eV the absolute photoionization cross-section of methyl radical was reported to be σ_{CH_3} (11.0 eV) = 6 ± 1.8 Mb.[48] The large uncertainty in the methyl cross-section (a relative uncertainty of 30% at 11 eV) is the dominant contributor to the uncertainty limits for the individual measurements of the methyl to acetylene ratio. Another measurement of the photoionization cross-section of methyl radical by Gans et al.[72] reports similar values and uncertainties to those measured by Taatjes et al.[48]

The remaining fraction of 12% at 950 K is then assumed to be in the form of the radical intermediate 2-furanyloxy. Results from the pressure-dependent plug flow reactor simulations using the kinetic mechanism in Table 2 (with the reactor exterior wall held at 950 K and an initial reactant concentration of 0.005% methoxyfuran in He) predict that the ratio of 2-furanyloxy to methyl radical at the exit to the reactor is 16% when Reaction 1 is as documented in Table 2.

Table 3: Measured ratio of HCCH to CH_3; observed ion signals for 0.005% methoxyfuran in He at 950 K and photoionization cross-sections (Mb) of CH_3[48] and HC≡CH.[49]

eV†	m/z 15 (counts)*	σ(CH_3)	m/z 26 (counts)*	σ(HCCH)	Ratio 26/15
11.40	4027	5.9	11840	15.3	0.86 ± 0.26
11.45	3906	6.8	14500	18.1	1.06 ± 0.32
11.50	3589	4.4	14630	18.3	0.74 ± 0.23
11.95	3944	5.5	24570	28.0	0.93 ± 0.28
12.00	4362	5.3	26490	28.1	0.87 ± 0.27
12.05	4642	5.8	26960	28.5	0.90 ± 0.28
					Average = 0.88 ± 0.27

†No values of σ(CH_3) reported between 11.5 and 11.95 eV

*Raw counts, baseline corrected only

When the A-factor of Reaction 1 is doubled (as in Figure 14), the predicted ratio of these radicals drops to 12%, which agrees very well with experimental observations.

A final quantified measurement is the amount of bimolecular chemistry observed at different experimental conditions. The two most abundant secondary products detected by both PIMS and infrared spectroscopy are acrolein (CH_2=CH-CHO) and crotonaldehyde (CH_3-CH=CH-CHO). The amount of these species are estimated in the same manner as described above for the ratio of acetylene to methyl radical in Eq. (4). In general, the formation of secondary products observed is small, approximately $1-3\%$ depending on the reactant concentration. The measured ratio of acrolein (m/z 56) to methyl radical at 950 K is $1.3 \pm 0.6\%$ and $1.5 \pm 0.7\%$ for mixtures of 0.005% and 0.01% methoxyfuran in He, respectively. Observations of crotonaldehyde relative to methyl are similar at 950 K, with ratios of $0.7 \pm 0.4\%$ and $1.9 \pm 0.9\%$ for mixtures of 0.005% and 0.01% methoxyfuran in He, respectively. For the purpose of this calculation the ion signal at m/z 70 is assumed to be entirely crotonaldehyde and the ratios calculated using the appropriate photoionization cross-section of both species.[49,54]

Simulations using the kinetic mechanism in Table 2 show that the amount of intermediates that could produce the final product species acrolein and crotonaldehyde, amount to about 2.5% and 0.001% relative to methyl radical, respectively. The mechanism accurately accounts for the amount of acrolein observed, but under predicts formation of CH_3 radical chemistry by about two orders

of magnitude compared to experimental observations. This suggests reactions with 2-furanyloxy are likely faster than the model predicts.

In general, the total formation of secondary products is small, accounting for about 3% of total methoxyfuran decomposition at the conditions studied with the remainder of decomposition following the unimolecular reaction in Scheme 2. Predictions using the kinetic model confirm the formation of intermediates from CH_3 or H addition reactions and reactions with 2-furanyloxy at the temperatures and residence times in the microreactor. Moreover, they offer a valid explanation for the species observed that are not included in the unimolecular reaction scheme.

Conclusions

The unimolecular thermal decomposition scheme of 2-methoxyfuran predicted computationally by Simmie et al.[3] is confirmed experimentally in a microreactor operated at $300-1300$ K, pressures up to 200 Torr and a residence time of $50-100$ μs. The primary products detected by photoionization time-of-flight mass spectrometry and FT-IR spectroscopy in an Ar matrix include CH_3, 2-furanyloxy, CO and HC≡CH. Secondary products resulting from H or CH_3 addition to 2-methoxyfuran and radical-radical reactions with 2-furanyloxy have also been detected and include CH_2=CH-CHO, CH_3-CH=CH-CHO, CH_3-CO-CH=CH_2 and furanones; quantification of the ion signal of these species indicates secondary reactions in a continuous flow reactor contribute to approximately 3% of total methoxyfuran consumption under the conditions studied. Results of calculations with a pressure-dependent kinetic mechanism show that experimental measurements are in general agreement with predictions and also provides plausible pathways for the observed bimolecular products.

Finally, for the first time the allylic lactone, 2-furanyloxy radical, was identified experimentally and characterized by PIMS and IR spectroscopy. The carbonyl stretch (ν_4) and several other infrared vibrational bands were assigned in an Ar matrix in addition to the ionization threshold and photoionization efficiency curve. Infrared and mass spectral evidence suggests that the life-

time of this radical is long enough to react with other radicals and contribute to the observation of secondary products. The apparent stability of this radical, at least in the pressure and temperature regimes examined, could have potential implications for the combustion of other structurally similar furanic fuels.

Acknowledgement

We acknowledge the United States Department of Energy (grant: DE-FG02-93ER14364), the U.S. DOE's Office of the Biomass Program (contract: 1544759) and the National Science Foundation (CHE-0848606 and CHD-1112466) for support of KNU, JWD and GBE. KNU specifically thanks Dr. Adam Scheer for photodiode measurements in addition to the most up-to-date photoionization cross-section data. MA, TPT and the Advanced Light Source are supported by the Director, Office of Energy Research, Office of Basic Energy Sciences and the Chemical Sciences Division of the U.S. Department of Energy (contract: DE-AC02-05CH11231). JMS thanks Dr. Kieran Somers for discussions on mechanistic aspects and the Irish Centre for High-End Computing (ICHEC) for the provisions of computational resources.

Supporting Information Available

Additional mass and infrared spectra are available in the Supporting Information.

This material is available free of charge via the Internet at `http://pubs.acs.org/`.

Notes and References

(1) (a) Haro, P.; Ollero, P.; Villanueva Perales, A.; Vidal-Barrero, F. *Biofuels, Bioproducts and Biorefining* **2013**, *7*, 551–572; (b) Lange, J.-P.; van der Heide, E.; van Buijtenen, J.; Price, R. *ChemSusChem* **2012**, *5*, 150–166; (c) Dutta, S.; De, S.; Saha, B. *Biomass and Bioenergy* **2013**, *55*, 355–369; (d) van Putten, R.-J.; van der Waal, J. C.; de Jong, E.; Rasrendra, C. B.; Heeres, H. J.; de Vries, J. G. *Chemical Reviews* **2013**, *113*, 1499–1597.

(2) Bruinsma, O.; Tromp, P.; de Sauvage Nolting, H.; Moulijn, J. *Fuel* **1988**, *67*, 334–340.

(3) Simmie, J.; Somers, K.; Yasunaga, K.; Curran, H. *International Journal of Chemical Kinetics* **2013**, *45*, 531–541.

(4) ex. $DH_{298}(CH_3O{-}CH_3)$ = 349 $\pm$ 3 kJ mol^{-1} and $DH_{298}(C_6H_5O{-}CH_3)$ = 258 $\pm$ 1.3 kJ mol^{-1}.

(5) Hudzik, J.; Bozzelli, J. *Journal of Physical Chemistry A* **2010**, *114*, 7984–7995.

(6) Barckholtz, C.; Fadden, M. J.; Hadad, C. M. *Journal of Physical Chemistry A* **1999**, *103*, 8108–8117.

(7) Tokmakov, I.; Kim, G.-S.; Kislov, V.; Mebel, A.; Lin, M. *Journal of Physical Chemistry A* **2005**, *109*, 6114–6127.

(8) Yamamoto, Y.; Ohno, M.; Eguchi, S. *Journal of Organic Chemistry* **1996**, *61*, 9264–9271.

(9) Guan, Q.; Urness, K.; Ormond, T.; Ellison, G.; Daily, J. *International Reviews in Physical Chemistry* **2014**, *33*, 447–487.

(10) Potential sources of error for measuring the temperature of the SiC reactor include: (a) An accuracy of 1%, as listed by the thermocouple (TC) manufacturer. (b) Imperfect thermal contact between the TC and reactor; this is difficult to quantify but is unlikely to be the dominant factor since most of the heat transfer is expected to be radiative at the upper temperatures. (c) Cooling along the TC wire away from the TC junction and point of contact with SiC reactor; probably a dominant factor and is likely on the order of 10s of °C. (d) Radiative losses from the surface area added by the TC. (e) The TC cold junction is at the vacuum feedthrough and not at the meter, where it would be properly compensated, resulting in an additional error of a few °C.

(11) Scheer, A.; Mukarakate, C.; Robichaud, D.; Nimlos, M.; Carstensen, H.-H.; Ellison, G. *Journal of Chemical Physics* **2012**, *136*, 044309.

(12) Urness, K. N.; Guan, Q.; Golan, A.; Daily, J. W.; Nimlos, M. R.; Stanton, J. F.; Ahmed, M.; Ellison, G. B. *Journal of Chemical Physics* **2013**, *139*, 124305.

(13) Vasiliou, A.; Piech, K.; Reed, B.; Zhang, X.; Nimlos, M.; Ahmed, M.; Golan, A.; Kostko, O.; Osborn, D.; David, D.; Urness, K.; Daily, J.; Stanton, J.; Ellison, G. *Journal of Chemical Physics* **2012**, *137*, 164308.

(14) Frisch, M. J. et al. Gaussian-09. Wallingford, CT 2009.

(15) Montgomery, J. A.; Frisch, M. J.; Ochterski, J. W.; Petersson, G. A. *Journal of Chemical Physics* **1999**, *110*, 2822–2827.

(16) Zhao, Y.; Truhlar, D. G. *Theoretical Chemistry Accounts* **2008**, *120*, 215–241.

(17) (a) Fukui, K. *Accounts of Chemical Research* **1981**, *14*, 363–368; (b) Hratchian, H. P.; Schlegel, H. B. *Journal of Chemical Theory and Computation* **2005**, *1*, 61–69.

(18) Curtiss, L. A.; Raghavachari, K.; Redfern, P. C.; Rassolov, V.; Pople, J. A. *Journal of Chemical Physics* **1998**, *109*, 7764–7776.

(19) Ochterski, J. W.; Petersson, G. A.; Montgomery, J. A. *Journal of Chemical Physics* **1996**, *104*, 2598–2619.

(20) Beukes, J.; Marstokk, K.-M.; Møllendal, H. *Journal of Molecular Structure* **2001**, *567-568*, 19–27.

(21) The one standard deviation uncertainty of the three methods for the adiabatic ionization energies for all reported species is between 0.02 to 0.09 eV.

(22) Lide, D., Ed. *CRC Handbook of Chemistry and Physics*; CRC Press, 1992.

(23) Blush, J.; Chen, P.; Wiedmann, R.; White, M. *Journal of Chemical Physics* **1993**, *98*, 3557–3559.

(24) Signorell, R.; Merkt, F. *Journal of Chemical Physics* **1999**, *110*, 2309–2311.

(25) Pratt, S.; Dehmer, P.; Dehmer, J. *Journal of Chemical Physics* **1993**, *99*, 6233–6244.

(26) Lau, K.-C.; Ng, C.-Y. *Accounts of Chemical Research* **2006**, *39*, 823–829.

(27) Evans, M.; Ng, C. *Journal of Chemical Physics* **1999**, *111*, 8879–8891.

(28) Mayer, E.; Grant, E. *Journal of Chemical Physics* **1995**, *103*, 10513–10519.

(29) Schulenburg, A.; Meisinger, M.; Radi, P.; Merkt, F. *Journal of Molecular Structure* **2008**, *250*, 44–50.

(30) Van Dam, H.; Oskam, A. *Journal of Electron Spectroscopy and Related Phenomena* **1978**, *13*, 273–290.

(31) Masclet, P.; Mouvier, G. *Journal of Electron Spectroscopy and Related Phenomena* **1978**, *14*, 77–97.

(32) Willett, G. D.; Baer, T. *Journal of the American Chemical Society* **1980**, *102*, 6769–6773.

(33) Terlouw, J. K.; Burgers, P. C.; Holmes, J. L. *Journal of the American Chemical Society* **1979**, *101*, 225–226.

(34) Watanabe, K. *Journal of Chemical Physics* **1957**, *26*, 542–547.

(35) (a) Terlouw, J.; Heerma, W.; Holmes, J.; Burgers, P. *Organic Mass Spectrometry* **1980**, *15*, 582–586; (b) Morizur, J.-P.; Mercier, J.; Sarraf, M. *Organic Mass Spectrometry* **1982**, *17*, 327–330.

(36) Würmel, J.; Simmie, J. *Journal of Physical Chemistry A* **2014**, *118*, 4172–4183.

(37) Wang, D.; Wang, D.; Li, S.; Li, Y. *Journal of Electron Spectroscopy and Related Phenomena* **1994**, *70*, 167–172.

(38) Zheng, S.; Wang, X.; Meng, L.; Cao, X.; Wang, D. *Science in China (Series B)* **1997**, *40*, 657–662.

(39) Klapstein, D.; MacPherson, C.; O'Brien, R. *Canadian Journal of Chemistry* **1990**, *68*, 747–754.

(40) Thorstad, O.; Undheim, K.; Cederlund, B.; Hörnfeldt, A.-B. *Acta Chemica Scandinavica B* **1975**, *29*, 647–651.

(41) Czekner, J.; Taatjes, C.; Osborn, D.; Meloni, G. *International Journal of Mass Spectrometry* **2013**, *348*, 39–46.

(42) Anderson, J. B.; Andres, R. P.; Fenn, J. B. *Advances in Chemical Physics: Supersonic Nozzle Beams*; Wiley-Interscience: New York, 1966; Vol. 10; Chapter 8, pp 275–317.

(43) Reaction Design, *Chemkin-Pro 15113*. San Diego, CA, 2012.

(44) The formyl vinyl radical can decompose by either an endothermic β-scission to acetylene (HC≡CH) and formyl radical (HCO) or a 1,3-H-shift to acryloyl (1-oxo-2-propen-1-yl or O=C-CH=CH_2). In the first case, a zero-point corrected electronic energy barrier of 117 kJ mol^{-1} must be surmounted, in the second case the barrier is 122 kJ mol^{-1}. The acryloyl radical itself then dissociates to CO and vinyl radical (CH_2=CH), with a barrier of 97 kJ mol^{-1}, a calculated value which is in excellent agreement with the experimentally determined velocity map imaging value of 96.2 $\pm$ 8.4 kJ mol^{-1} by Lau et al.[73] and their high-level CCSD(T)/aug-cc-pV(Q+d)Z calculations of 98.3 kJ mol^{-1} (for a more nuanced discussion of the structural properties of the acryloyl radicals, see the work by Cooksy.[74]).

(45) Dissociative photoionization refers to ionization and subsequent ion fragmentation of a vibrationally excited species to a cation and a neutral; in the case of 2-methoxyfuran: 2-MeOF* + $\hbar\omega_{\mathrm{VUV}} \rightarrow$ [2-MeOF$^+$]* $\rightarrow$ products.

(46) Bieri, G.; Burger, F.; Heilbronner, E.; Maier, J. *Helvetica Chimica Acta* **1977**, *60*, 2213–2233.

(47) Engdahl, A.; Nelander, B. *Chemical Physics Letters* **1983**, *100*, 129–132.

(48) Taatjes, C.; Osborn, D.; Selby, T.; Meloni, G.; Fan, H.; Pratt, S. *Journal of Physical Chemistry A* **2008**, *112*, 9336–9343.

(49) Cool, T.; Wang, J.; Nakajima, K.; Taatjes, C.; McIlroy, A. *International Journal of Mass Spectrometry* **2005**, *247*, 18–27.

(50) Breda, S.; Reva, I.; Fausto, R. *Journal of Molecular Structure* **2008**, *887*, 75–86.

(51) Blom, C.; Müller, R.; Günthard, H. *Chemical Physics Letters* **1980**, *73*, 483–486.

(52) Johnstone, D.; Sodeau, J. *Journal of the Chemical Society-Faraday Transactions* **1992**, *88*, 409–415.

(53) Goulay, F.; Trevitt, A.; Savee, J.; Bouwman, J.; Osborn, D.; Taatjes, C.; Wilson, K.; Leone, S. *Journal of Physical Chemistry A* **2012**, *116*, 6091–6106.

(54) Yang, B.; Wang, J.; Cool, T.; Hansen, N.; Skeen, S.; Osborn, D. *International Journal of Mass Spectrometry* **2012**, *309*, 118–128.

(55) Goulay, F.; Derakhshan, A.; Maher, E.; Trevitt, A.; Savee, J.; Scheer, A.; Osborn, D.; Taatjes, C. *Physical Chemistry Chemical Physics* **2013**, *15*, 4049–4058.

(56) Urness, K. N. A molecular picture of biofuel decomposition: Pyrolysis of furan and select furanics. PhD, University of Colorado at Boulder, 2014.

(57) Würmel, J.; Simmie, J. *To be submitted* **2015**,

(58) Xu, Z.; Mok, C.; Chin, W.; Huang, H.; Li, S.; Huang, W. *Journal of the Chemical Society, Perkin Transactions 2* **1999**, 725–729.

(59) Casarini, D.; Lunazzi, L.; Placucci, G.; Venturini, A. *Journal of Organic Chemistry* **1991**, *56*, 414–417.

(60) Mulcahy, M.; Tucker, B.; Williams, D.; Wilmshurst, J. *Chemical Communications* **1965**, 609–610.

(61) Mulcahy, M.; Tucker, B.; Williams, D.; Wilmshurst, J. *Australian Journal of Chemistry* **1967**, *20*, 1155–1171.

(62) Holbrook, K. A.; Pilling, M. J.; Robertson, S. H. *Unimolecular Reactions*, 2nd ed.; Wiley: England, 1996; Chapter 3.

(63) Mokrushin, V.; Tsang, W. ChemRate version 1.5.8, NIST, Gaithersburg, MD 20899. `http://mokrushin.com/ChemRate/chemrate.html`, accessed June 21 2013.

(64) Somers, K. P.; Simmie, J. M.; Metcalfe, W. K.; Curran, H. J. *Physical Chemistry Chemical Physics* **2014**, *16*, 5349–5367.

(65) (a) Wang, H.; You, X.; Joshi, A. V.; Davis, S. G.; Laskin, A.; Egolfopoulos, F.; Law, C. K. USC Mech Version II. High-Temperature Combustion Reaction Model of H_2/CO/C_1-C_4 Compounds. 2007; `http://ignis.usc.edu/USC_Mech_II.htm`; (b) Li, J.; Zhao, Z.; Kazakov, A.; Dryer, F. L. *International Journal of Chemical Kinetics* **2004**, *36*, 566–575; (c) Li, J.; Zhao, Z.; Kazakov, A.; Chaos, M.; Dryer, F. L.; J. J. Scire, Jr., *International Journal of Chemical Kinetics* **2007**, *39*, 109–136; (d) Tian, Z.; Yuan, T.; Fournet, R.; Glaude, P.-A.; Sirjean, B.; Battin-Leclerc, F.; Zhang, K.; Qi, F. *Combustion and Flame* **2011**, *158*, 756–773; (e) Baulch, D. L.; Cobos, C. J.; Cox, R. A.; Esser, C.; Frank, P.; Just, T.; Kerr, J. A.; Pilling, M. J.; Troe, J.; Walker, R. W.; Warnatz, J. *Journal of Physical and Chemical Reference Data* **1992**, *21*, 411–734.

(66) Tsang, W.; Hampson, R. *Journal of Physical and Chemical Reference Data* **1986**, *15*, 1087–1279.

(67) Krasnoperov, L.; Chesnokov, E.; Stark, H.; Ravishankara, A. *Journal of Physical Chemistry A* **2004**, *108*, 11526–11536.

(68) Baulch, D. L.; Cobos, C. J.; Cox, R. A.; Frank, P.; Hayman, G.; Just, T.; Kerr, J. A.; Murrells, T.; Pilling, M. J.; Troe, J.; Walker, R. W.; Warnatz, J. *Journal of Physical and Chemical Reference Data* **1994**, *23*, 847–1033.

(69) Liu, D.; Togbé, C.; Tran, L.-S.; Felsmann, D.; Oßwald, P.; Nau, P.; Koppmann, J.; Lackner, A.; Glaude, P.-A.; Sirjean, B.; Fournet, R.; Battin-Leclerc, F.; Kohse-Höinghaus, K. *Combustion and Flame* **2014**, *161*, 748–765.

(70) (a) Somayajulu, G. R. *Journal of Chemical and Engineering Data* **1989**, *34*, 106–120; (b) Wang, H.; Frenklach, M. *Combustion and Flame* **1994**, *96*, 163–170.

(71) Ormond, T. K.; Scheer, A. M.; Nimlos, M. R.; Robichaud, D. J.; Troy, T. P.; Ahmed, M.; Daily, J. W.; Nguyen, T. L.; Stanton, J. F.; Ellison, G. B. *Journal of Physical Chemistry A accepted Jan 2015*.

(72) Gans, B.; Mendes, L. V.; Boyé-Péronne, S.; Douin, S.; Garcia, G.; Soldi-Lose, H.; de Miranda, B. C.; Alcaraz, C.; Carrasco, N.; Pernot, P.; Gauyacq, D. *Journal of Physical Chemistry A* **2010**, *114*, 3237–3246.

(73) Lau, K.-C.; Liu, Y.; Butler, L. *Journal of Chemical Physics* **2005**, *123*, 054322.

(74) Cooksy, A. L. *Journal of Physical Chemistry A* **1998**, *102*, 5093–5099.

Graphical TOC Entry